JOURNAL OF GEOPHYSICAL RESEARCH, VOL. 114, B10303, doi:10.1029/2008JB006118, 2009

Inferring the coseismic and postseismic stress changes caused by the 2004 M_w = 6 Parkfield earthquake from variations of recurrence times of microearthquakes

O. Lengliné[1] and D. Marsan[1]

Received 26 September 2008; revised 2 June 2009; accepted 30 June 2009; published 1 October 2009.

[1] Kinematic models of coseismic stress, inverted from ground motion data, do not usually find good correlation between the location of aftershocks and high-stress patches. In particular, numerous earthquakes are recorded in areas of the fault where the stress decreases. However, most of coseismic slip distributions have limited spatial resolution (typically not better than ~1 km). Here we investigate the stress changes produced by the 2004 M_w = 6 Parkfield earthquake on and near its rupture zone, at the scale of magnitude 2 earthquake asperities (approximately tens of meters). After relocating earthquakes in this zone between 1984 and 2007, we form repeating, highly similar earthquake sequences and study how the quasiperiodicity of occurrence at each sequence, observed during the 20 years preceding the 2004 main shock, is perturbed by this event. We apply a simple model of the seismic cycle to infer the coseismic and postseismic stresses experienced by the repeatedly failing asperities. Despite being spatially sparse, these stress distributions have resolutions only limited by the typical scale of an asperity. We propose that the high spatial variability of the seismicity patterns following the M_w = 6 earthquake, results from an heterogeneous coseismic stress field. The emergence of the Omori-Utsu law observed at large-scale (greater than kilometers) at Parkfield is simply the outcome of averaging such quasi-deterministic patterns over many sequences. The fact that the coseismic stress can significantly change over distances of the order of 100 m adds credence to the hypothesis that earthquake rupture is intrinsically very heterogeneous.

Citation: Lengliné, O., and D. Marsan (2009), Inferring the coseismic and postseismic stress changes caused by the 2004 M_w = 6 Parkfield earthquake from variations of recurrence times of microearthquakes, *J. Geophys. Res.*, *114*, B10303, doi:10.1029/2008JB006118.

1. Introduction

[2] Decay of the body wave displacement spectrum at high frequencies has been suggested as the signature of coseismic slip heterogeneities on the fault plane [*Andrews*, 1980; *Frankel*, 1991]. The typical ω square slope of this far-field displacement spectrum is interpreted as the result of the self-similarity of earthquake rupture [*Herrero and Bernard*, 1994]. Slip heterogeneities are also evidenced by inversion of seismic waves [e.g., *Bouchon*, 1997], with typically one or several large slip asperities embedded in a low slip zone. However, kinematic rupture models are restricted to long wavelength (typically <1 Hz), as high-frequency radiations are too complex to model. Although the stress field is supposed to be self-similar, and therefore heterogeneous at all scales, its estimation is thus limited to the largest scales, hence ignoring the largest stress variations that are expected to characterize the small scales (<1 km). Slip distributions measured from earthquake surface rupture also attest for a highly variable coseismic slip. This strong variability was observed for example for the Izmit 1999 earthquake [*Barka et al.*, 2002], and is typical of many other earthquakes [*Manighetti et al.*, 2005]. *Schmittbuhl et al.* [2006] proposed that the Nojima fault, in Japan, exhibits a strong shear stress spatial variability and that this heterogeneity results from the geometry of the fault.

[3] The existence of an heterogeneous stress field accompanying earthquake rupture has important implications for the location of future earthquakes [e.g., *Beroza*, 1991; *Parsons*, 2008], and more generally on regional-scale seismicity patterns. *Marsan* [2006] and *Helmstetter and Shaw* [2006] used a stochastic slip distribution to model the slip distribution caused by an earthquake, coupled with a rate and state friction model for reproducing the nucleation process of subsequent earthquakes. These models can explain why seismic quiescences are commonly not observed in stress shadows, although these quiescences are predicted by simple, smooth homogeneous dislocation models. In particular it was shown that most of the seismicity is controlled by small, highly localized fault patches experiencing the highest stress changes. Furthermore, the control of seismicity (and, in particular, of aftershocks) by small-scale heterogeneities might explain the absence of

[1]Laboratoire de Géophysique Interne et Tectonophysique, CNRS, Université de Savoie, France.

0148-0227/09/2008JB006118$09.00

correlation between aftershock distribution and slip/stress inversions (see *Das and Henry* [2003] for a review). However, the models of *Marsan* [2006] and *Helmstetter and Shaw* [2006] are simplified in the sense that they consider the main shock rupture to be independent of the location of potential earthquake nucleation sites, which may not be the case.

[4] It has been proposed to quantify the coseismic stress drop variability on the fault plane by the temporal evolution of the average seismicity produced on this fault plane [*Helmstetter and Shaw*, 2006; *Marsan and Daniel*, 2007; *Peng et al.*, 2007]. However, the effect of stress drop variability on seismicity is the clearest at short timescale following the main rupture, i.e., when the main rupture is just finished and the aftershock productivity is at its highest. The heterogeneity of the stress drop is therefore difficult to constrain from the aftershock time series as many aftershocks are missed at these short times scales [*Kagan*, 2004]. Several attempts have been performed to estimate seismicity rates from the first minute onward following a main shock [*Peng et al.*, 2006, 2007]. However, even when incorporating these early aftershocks, the heterogeneity of the stress drop remains difficult to constrain.

[5] This manuscript describes an original attempt at detecting coseismic stress variations on the main fault by using aftershock data. Our approach is different from the one proposed by *Marsan* [2006] and *Helmstetter and Shaw* [2006] in the sense that instead of looking at an average, large-scale ($\sim$10 km) effect of stress heterogeneity on the resulting seismicity, we investigate the coseismic stress variation at the scale ($\sim$10 m) of a microearthquake asperity. We analyze microearthquakes occurrences in the Parkfield area of the San Andreas fault system from 1984 to 2007. After relocating earthquakes and forming earthquake repeating sequences on the basis of waveform similarity, we show that seismic slip on most individual earthquake asperities occurs in a remarkably periodic fashion during the interseismic period [*Nadeau et al.*, 1995; *Nadeau and McEvilly*, 1997, 1999]. We then exploit this periodicity by analyzing how it is perturbed by the 2004 Parkfield, $M_w = 6$ earthquake. This enables us to quantify the spatial variation on $\sim$10 m size asperities of the stress caused by the main shock rupture. Although the resulting stress field estimate is very sparse, its spatial resolution is only limited by the typical scale of an asperity.

2. Tectonic Setting

[6] We examine the seismicity on the Parkfield segment of the San Andreas fault system. At its southern end, this segment is bounded by a locked section which last ruptured during the 1857 Fort Tejon earthquake [*Sieh*, 1978]. On the contrary, the northern end is freely slipping at 2.5 cm a^{-1} at shallow depth [*Harris and Segall*, 1987; *Murray et al.*, 2001]. Interseismic slip velocity gradually decreases between these two bounds. Although the slip speed varies spatially along the fault, it remained approximately steady for at least 35 years [*Titus et al.*, 2006]. However, transient, small, localized aseismic deformations are also observed on the fault plane [*Murray and Segall*, 2005], and may impact the seismicity dynamics [*Nadeau and McEvilly*, 1999]. The Parkfield area appears relatively insensitive to stress transients driven by seismic waves originating from remote ruptures [*Hill et al.*, 1993]. The only significant earthquake that occurred in the studied interval (apart from the 2004 $M_w = 6$ Parkfield earthquake) is the 2003 San Simeon earthquake which did not cause any significant effect on the Parkfield seismicity [*Hardebeck et al.*, 2004]. The last earthquakes which had a significant impact on Parkfield seismicity were the 1983 Coalinga-Nuñez earthquakes [*Toda and Stein*, 2002]; hence, a year before the beginning of the interval we study in this work.

[7] The Parkfield segment experienced four $M_w \sim 6$ earthquakes since 1922 (1922, 1934, 1966, 2004). All these earthquakes have a similar magnitude, rupture extent and focal mechanism. Although these earthquakes have different hypocenters, they are considered as repeating earthquakes as it is hypothesized that they have similar rupture zones [*Bakun and McEvilly*, 1984; *Bakun et al.*, 2005]. The last earthquake of this $M_w \sim 6$ sequence occurred on the 28 September 2004. It produced a maximum coseismic slip of 40–50 cm at depth and a significant postseismic displacement, which total moment exceeded the coseismic moment by a factor of almost 2 after 2 months [*Langbein et al.*, 2006]. Repeating earthquake sequences are not limited to $M_w \sim 6$ earthquakes and were also evidenced in the Parkfield transition area for smaller magnitudes [*Nadeau et al.*, 1995; *Waldhauser et al.*, 2004]. Relocated seismicity highlights the fact that repeating sequences are not homogeneously distributed along the fault plane but are rather strongly clustered, typically collapsing into subhorizontal streaks [e.g., *Rubin et al.*, 1999; *Schaff et al.*, 2002; *Waldhauser et al.*, 2004]. At Parkfield, these seismicity streaks are thought to bound a locked area where most of the coseismic slip of the 1966 and 2004 earthquakes took place [*Waldhauser et al.*, 2004; *Thurber et al.*, 2006].

3. Data and Processing

3.1. Earthquake Relocation

[8] We select a $\sim$75-km-long segment of the San Andreas fault which encloses the 2004 $M_w = 6$ Parkfield earthquake rupture and its aftershocks (Figure 1). This portion of the San Andreas fault system is densely covered by Northern California Seismic Network (NCSN) stations. We select all earthquakes located less than 5 km away from the segment and that occurred between January 1984 and June 2007. Among this set of earthquakes, we only keep those with at least four available waveforms as recorded by NCSN, vertical component, short-period stations. These waveforms are sampled at 100 Hz and are archived at the Northern California Earthquake Data Center (NCEDC). We thus obtain a set of 12,230 earthquakes with a total of 164,152 waveforms.

[9] The cross-spectral method is used to perform both multiplet selection and time delay computation [*Jenkins and Watts*, 1968]. A 256-sample-long record (2.56 s) with 100 samples before the P wave arrival, is extracted from each waveform. Earthquakes are then linked together and organized in multiplets: two earthquakes are linked if their mean coherency computed for at least five stations on a 1.28-s-long window, centered on the P wave arrival, in the frequency interval [1.5–18] Hz, is greater than a given threshold. The coherency is defined as the smoothed cross-

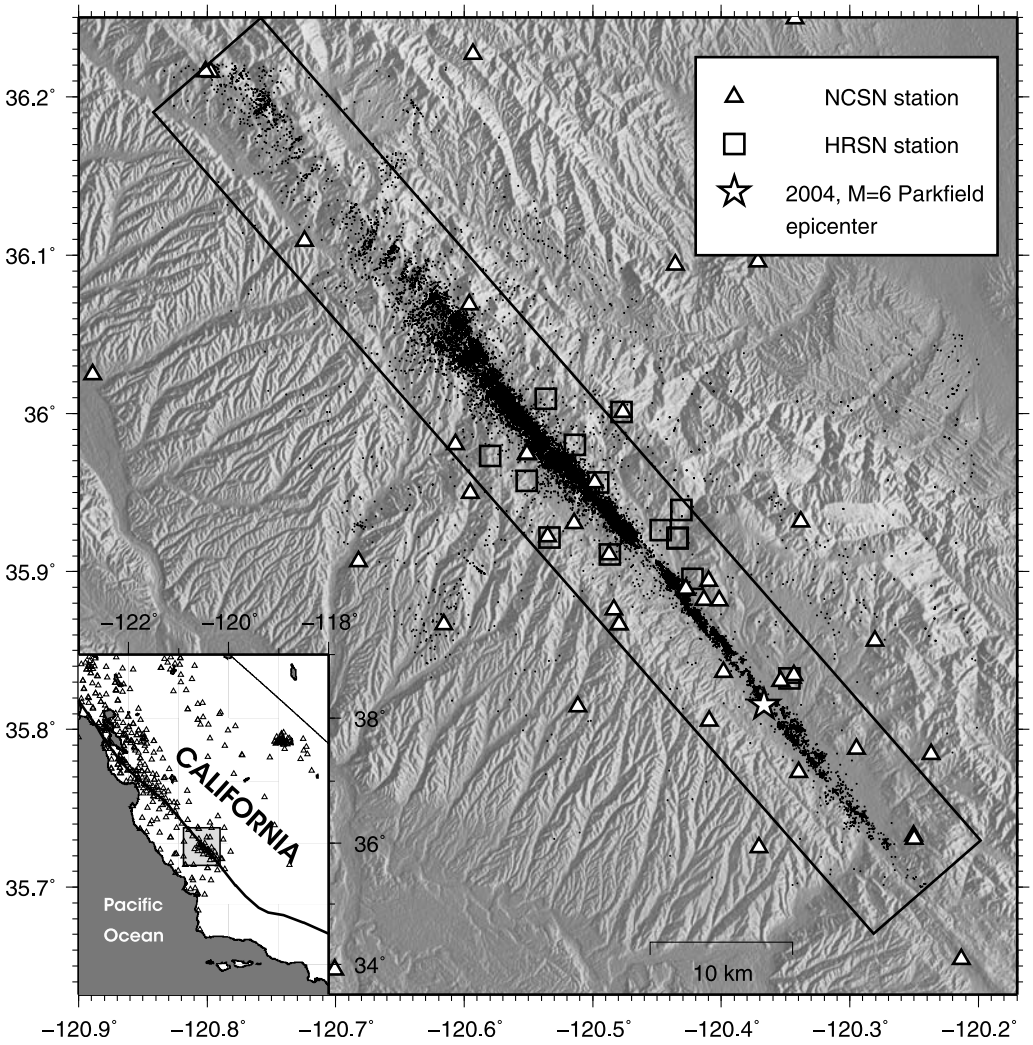

Figure 1. Map of the seismicity on the San Andreas fault near Parkfield. Black dots represent the epicenters of earthquakes that occurred in the studied interval (1984–2007). The rectangle denotes the selected area. Squares are High Resolution Seismic Network (HRSN) seismic stations, and triangles are NCSN seismic stations. The star shows the epicenter of the 2004 $M_w = 6$ earthquake. Inset map shows the location of the Parkfield area in California, on the San Andreas fault trace (shown as a thick line).

spectrum normalized by the smoothed autospectra of each windowed seismogram. We let this threshold vary between 85% and 95%. We use a smoothing function for spectra densities defined as the Fourier transform of a Tukey window of order 2. Time delays are then computed for all earthquakes pairs and for all common stations. These delays are computed in the frequency domain as it allows to obtain estimates with an accuracy better than the sampling period (10 ms). To do so, we follow an iterative approach, first computing the cross-spectrum between two waveforms, on a 128-sample-long window and then extracting its phase. This phase, weighted by the coherency, is finally fitted by a linear model between 1.5 and 20 Hz (see Figure 2). We impose this fit to pass through the origin. The estimated slope gives the time delay between the two windows. The two windows are aligned and we iterate the procedure until convergence is reached [*Got et al.*, 1994; *Got and Okubo*, 2003].

[10] Time delays are used to constrain locations and origin time shifts of each earthquake of a given multiplet (Figure 3). This step is performed by an iterative algorithm which progressively downweigh inconsistent data measurements [*Got and Okubo*, 2003]. A 1-D, P wave velocity model is required for this relocation process; we extract 1-D velocity profiles from the 3-D tomography of the Parkfield area performed by *Thurber et al.* [2006] and use the velocity profile that is the closest to the multiplet location. We finally convert relative relocations to absolute locations by imposing the barycenter of the original locations to be the barycenter of the relocated earthquakes for a multiplet. The final root-mean-square (RMS) arrival time residual is 12 ms, comparable to the 10 ms of *Thurber et al.* [2006] for cross-correlation data. Among the original set of 12,230 earthquakes, 8168 earthquakes are relocated with 4142 of them occurring before the 2004 $M_w = 6$ Parkfield earthquake (Figure 4).

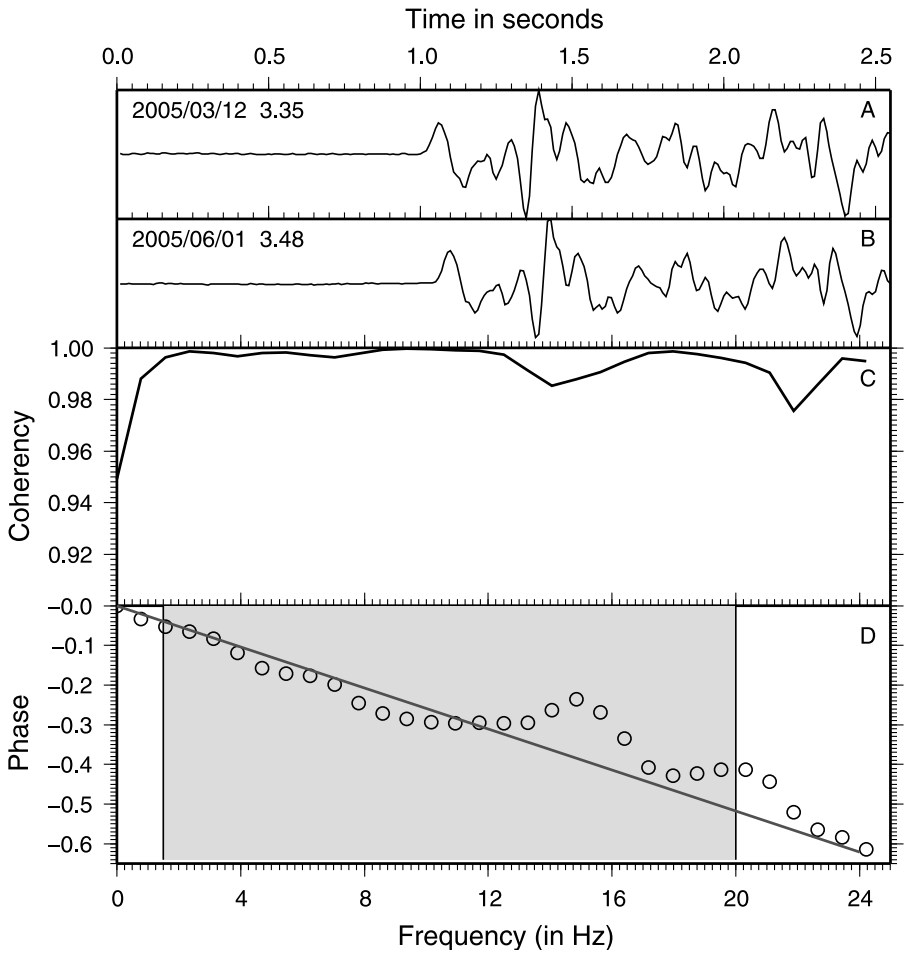

Figure 2. (a and b) Waveforms recorded at station PMM for two earthquakes of a common multiplet. Date and magnitude of each event are indicated in the upper left corner. (c) Coherency computed between the two waveforms. In this example, the coherency is very high, attesting for the high similarity between the two waveforms. (d) Phase of the cross spectrum computed for the waveforms in Figures 2a and 2b. Phase measurements (circles) are weighted at each frequency according to the coherency. A linear fit of the weighted phase is displayed as a black line. The fit is only performed in the frequency interval [1.5–20 Hz], as shown by the gray area. The time delay between the two earthquakes is given by the slope of the linear fit, here equal to 25.9 ms.

3.2. Forming Repeating Sequences

[11] Many relocated earthquakes have overlapping sources (e.g., Figure 3). These earthquakes ruptured the same asperity, and form what we call a repeating sequence. We thus identify sequences of repeating earthquakes, consisting of events with (1) identical rupture sizes, (2) identical recorded waveforms, and (3) overlapping sources. Previous studies based their identification of repeating sequences either on waveform similarity alone [*Nadeau et al.*, 1995; *Nadeau and McEvilly*, 1997], or according to criteria based on source overlap and magnitude difference. For example, *Waldhauser and Ellsworth* [2002] linked earthquakes that have more than 50% of source overlap and magnitude difference less than 0.5. Here, we consider that two earthquakes belong to the same repeating sequence if (1) their mean coherency in the [1.5–18 Hz] band is greater than 90%, (2) if the source overlap between the two earthquakes is greater than 70% in the horizontal direction and 35% in the vertical direction, and (3) if the difference of magnitude is less or equal to 0.2. We assume a circular rupture for all earthquakes, where the rupture radius, r (in km) is derived for a constant mean stress drop, $\Delta\sigma$, of about 3 MPa, using the relation linking earthquake radius and moment $r = \left(\frac{7M_0}{16\Delta\sigma}\right)^{1/3}$, with M_0 the seismic moment [*Eshelby*, 1957]. The seismic moment is obtained using the duration magnitude–seismic moment relation found by *Bakun* [1984] for earthquakes in central California.

[12] We do not impose the same source overlap requirement in the vertical and in the horizontal directions, in order to take into account a better performance of the relocation process along the horizontal direction. We also impose that a repeating sequence must be composed of earthquakes with at least half of them having a magnitude greater than the magnitude of completeness, m_c, estimated to be $m_c = 1.2$. This set of criterion A leads to the formation of 4325 sets but most of these sets only have one single event, while 334 repeating sequences (totaling 2414 earthquakes) have at least three events each. We also test how this grouping is dependent on our criteria by alternatively considering two

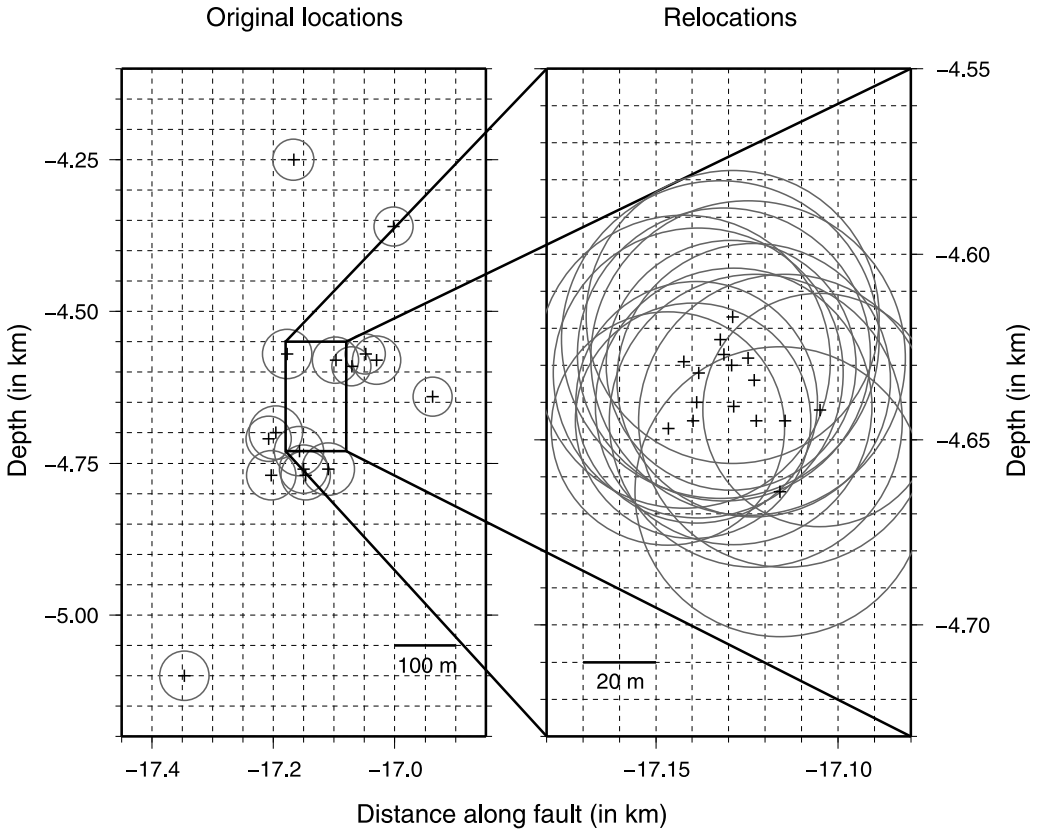

Figure 3. Example of the relocation process for a multiplet. (left) Cross section showing the original locations of the earthquakes. The inner rectangle denotes the area represented in Figure 3 (right). (right) Cross section of the relocated earthquakes. The circles give the approximate rupture dimension, assuming a constant mean stress drop of 3 MPa for all earthquakes and a circular rupture. Note that all relocated earthquakes in this multiplet have overlapping sources and very similar rupture sizes.

other sets of parameters: one corresponding to a relatively tight selection approach B and the other one to a relatively loose selection criterion C. Table 1 details the parameters used for the three selection sets. Selection A proposed is chosen as a good compromise between grouping too dissimilar earthquakes (which will possibly not belong to a common asperity) on the one hand, and a selection where too few earthquakes will remain due to uncertainties in the

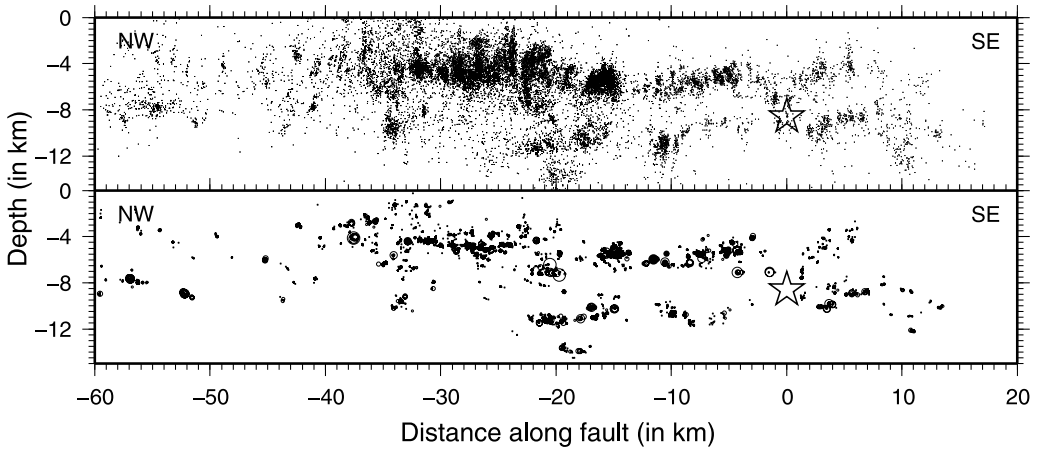

Figure 4. (top) Cross section of the seismicity along the San Andreas fault at Parkfield. Black dots are the original earthquake locations. The star shows location of the 2004 M_w = 6 hypocenter. (bottom) Relocated earthquakes. The circles give the earthquake rupture dimension, assuming a 3 MPa mean stress drop. The origin of the cross section is the location of the 2004 M_w = 6 Parkfield earthquake, and distances are positive in the SE direction.

Table 1. Details of the Parameters Used for Linking Two Earthquakes in Order to Build a Repeating Sequence[a]

Selection	Mean Coherency Threshold	Source Overlap in the Horizontal Direction	Δm	N^{1+}	N^{3+}	N_{eq}^{3+}
A (preferred)	90%	70%	0.2	4325	334	2414
B (tight)	95%	70%	0.2	5100	313	2098
C (loose)	90%	50%	0.5	3165	301	3058

[a]Selection A, B, and C refer to the preferred, the tight, and the loose set of parameters, respectively. The source overlap imposed in the vertical direction is half of what is required in the horizontal direction. The maximum difference of magnitude is noted Δm. N^{1+} is the number of sets with at least one earthquake. The number of sequences with at least three earthquakes is denoted by N^{3+} while the resulting number of earthquakes in these N^{3+} sequences is N_{eq}^{3+}. Note that the loose selection links more earthquakes together, but in a smaller number of sequences, resulting in repeating sequences with typically many more events than with the two other selections.

relocation, source geometries, and noise in the recorded waveforms, on the other hand.

3.3. Detection of Early Aftershocks of the 2004 Parkfield Earthquake

[13] It is likely that aftershocks of the 2004 $M_w = 6$ main shock are missing in the NCSN data set due to the high seismic activity in the first hours following this earthquake. The absence of early aftershocks is commonly observed even in densely covered areas but is believed to be mainly a detection problem [*Kagan*, 2004]. Working specifically on the aftershock sequence of the 2004 $M_w = 6$ Parkfield earthquake, [*Peng et al.*, 2006] found that numerous earthquakes were missed in the NCSN catalog at the time of their study. However, even after accounting for these missed events, an early aftershock deficiency was still observed during the first 132 *s* following the main shock initiation. Our goal is here not to detect all short-term aftershocks of the 2004, Parkfield earthquake, but only those which belong to previously identified repeating sequences or stand-alone events (sequence with only one earthquake).

[14] To complement the NCSN data set, we exploit the measurements performed by High Resolution Seismic Network (HRSN) stations (Figure 1). These stations have a good signal-to-noise ratio as they are installed in boreholes. We select the DP1 channel, which corresponds to the vertical component channel recording at 250 samples/sec. Our procedure for identifying early aftershocks can be decomposed in the following steps:

[15] 1. We extract the continuous signal on the DP1 channel for all HRSN stations for 24 h, with 1 h before and 23 h after initiation of the Parkfield 2004 event.

[16] 2. For each sequence previously formed we use the last earthquake of the sequence as the target event representative of the whole sequence. Recall that all earthquakes of a given sequence have very similar waveforms, hence the choice of the target event has little effect on this study. In order to work with the maximum number of sequences, we use the set of parameters of selection B, see Table 1 and hence 5100 target events. We then extract the corresponding waveforms on DP1 channel of HRSN stations for all the target events. Specifically, a 512-point-long window centered on the P wave is selected, for all HRSN stations. Unfortunately, it was not possible to obtain these waveforms for all target earthquakes as waveforms are not available for events that occurred before 2001. Among the 5100 sequences, 1542 sequences are without any waveform available for the target earthquake. A total of 1402 out of these 1542 sequences correspond to sequences with the last event occurring before March 2001.

[17] 3. We pass the waveform of the target event on the continuous record of each station. At each time step the target waveform and the continuous signal are aligned and the mean coherency between these two signals is computed in the frequency range 1.5 to 22.5 Hz. The target event window is then shifted by a tenth of the window length ($\sim$0.2 *s*) and a new coherency is computed. This gives the coherency versus time for a given station and sequence.

[18] 4. We compute the maximum coherency over a 6 s interval for all stations that recorded the target event. This is done to account for the propagation of the P wave between stations: a 6s interval ensures that all the HRSN stations can potentially have recorded the target earthquake. Finally, the maximum coherency for the target earthquake is averaged over all stations.

[19] 5. An aftershock is detected and associated to a repeating sequence if the final coherency, exceeds a certain threshold (Figure 5). We test three different coherency thresholds at 99%, 95%, and 90%.

[20] 6. Numerous detected events could not be linked to aftershocks listed in the NCSN data set. These new events are thus included in our repeating sequences. If a detection is associated to more than one repeating sequence, we include it in the repeating sequence characterized by the higher coherency.

[21] Figure 6 shows the aftershock rate for all sequences, when including the new detected events. The decay is best modeled by a power law when the 95% threshold is used. A p value of 0.71 is then found, in agreement with $p = 0.74$ obtained by *Peng et al.* [2006]. We therefore keep this 95% threshold for the remainder of this study.

4. Dynamics of Repeating Earthquakes During the Interseismic Stage

[22] We study the temporal patterns associated with repeating earthquake sequences. We focus on earthquakes that occurred before the 2004 $M_w = 6$ main shock and thus that were not perturbed by coseismic nor postseismic effects. For each repeating sequence with at least four earthquakes before the 2004 main shock, we define the mean interevent time ($\overline{T}_r$) as the mean of the time intervals, T_r, between two successive earthquakes. For each such sequence, we define the normalized interevent times as $T_r/\overline{T}_r$. Normalized interevent times, computed over all sequences, are then sorted by time bins. In order to obtain a probability density, the number of recurrence times falling in each time bins are then divided by the length of the time bin and the total number of normalized recurrence times. Figure 7 shows the probability density function of all the normalized times, for the three sets of selection parameters. Details concerning computation of uncertainties can be found in Appendix A.

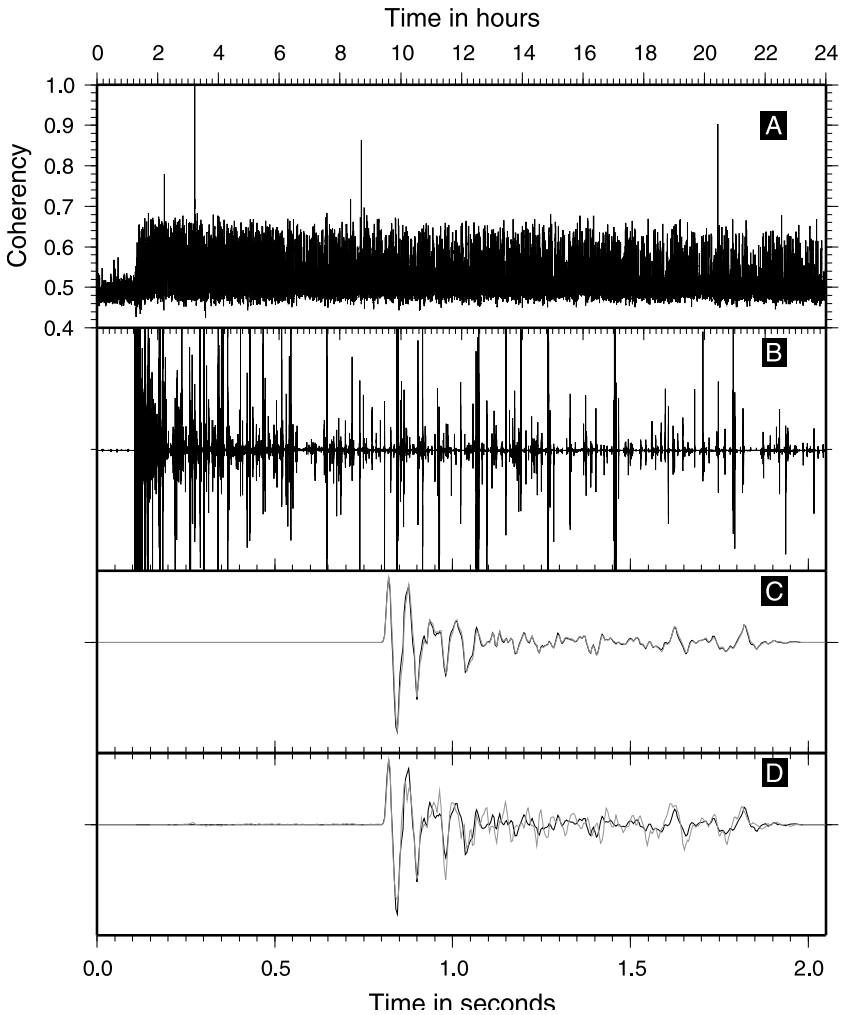

Figure 5. Details of the short-term earthquake detection process. (a) Maximum coherency computed over 24 h for an identified event and all HRSN recording stations, averaged over 6 s and over the stations. The 2004 $M_w = 6$ Parkfield earthquake occurred 1 h and 15 min after the beginning of the record and is associated with the coherency jump. The highest peak (3.2 h), with a coherency greater than 99% is associated with the detection of an aftershock not listed in the NCSN data set. (b) Continuous record on the DP1 channel of station CCR of the HRSN. The record is displayed over 24 h as represented in Figure 5a. An intense earthquake activity is visible on this record. (c) Waveform of the target event used for the detection (gray) and of the continuous signal (black) at the time of the highest coherency peak (∼3.2 h). The two waveforms recorded on the DP1 channel of station CCR are nearly identical, as expected given the very high coherency found at this time. (d) Same as Figure 5c, where the gray waveform correspond to the second coherency peak (∼8.5 h). The two waveforms are not as similar as in Figure 5c, and this event is not attached to the target sequence due a coherency below the threshold.

[23] A power law decay at short normalized times (up to 0.1) is visible for all selection sets. This decrease is similar to an Omori law decay of the number of aftershocks. Remarkably, a clear peak in the distribution is also observed close to unity, implying that the recurrence is quasiperiodic as long as $T_r/\overline{T}_r > 0.1$. This peak is mostly pronounced in distributions A and B: taking looser criteria (such as criterion C) implies mixing distinct asperities with distinct quasi-cycles, hence partly destroying the apparent quasiperiodicity of the sequences. It could therefore be expected that tighter and tighter criteria would lead to an even more obvious periodicity. The size of the data set does not, however, allow us to investigate this further.

[24] A clear distinction between two different behaviors is highlighted. At short normalized times ($T_r < 0.1 \times \overline{T}_r$), the dynamics of earthquakes is dominated by interactions between the asperities. However, the proportion of earthquakes involved in this interaction regime is low (∼5%). During this regime, the probability of an earthquake occurrence decreases with time as the interactions get weaker. The second regime ($T_r > 0.1 \times \overline{T}_r$) is driven by steady stress accumulation, and is characterized by the quasiperiodicity of earthquake recurrence times.

4.1. Periodicity

[25] We further investigate the second regime of repeating sequences, i.e., quasiperiodicity, previously identified by

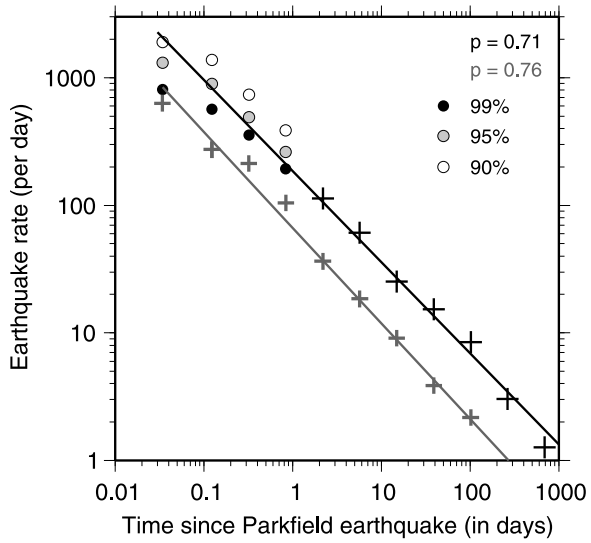

Figure 6. Earthquake rate computed for all earthquakes in our relocated catalog that followed the 2004 M_w = 6 Parkfield earthquake, including the new events detected in the first 23 h after the M_w = 6 earthquake. The circles with different levels of gray indicate the different coherency threshold used in the detection process. Black crosses are values not affected by the detection procedure (>23 h). The decay is best adjusted by a power law fit with an exponent p = 0.71 for the 95% coherency threshold. The gray crosses refer to the earthquake rate following the 2004 main shock computed only for repeating sequences with at least three earthquakes. A detection threshold of 95% is used and the decay is best adjusted by a power law fit with an exponent p = 0.76.

Nadeau et al. [1995], *Nadeau and McEvilly* [1997], *Nadeau and Johnson* [1998], and *Nadeau and McEvilly* [1999]. We compute the coefficient of variation for all repeating sequences with at least four events and which occurred before the 2004 M_w = 6 Parkfield earthquake. The coefficient of variation (COV) is the ratio, for a repeating sequence, of the standard deviation of T_r over the mean interevent time ($\overline{T}_r$). A COV of 0 implies a perfectly periodic recurrence while COV = 1 is characteristic of a Poisson (i.e., random) sequence. The COV values obtained for the three sets of parameters are mostly lower than 1 (see Figure 8), as expected in case of quasiperiodicity. This behavior can be interpreted as the result of a constant stressing rate acting on the asperities, in which case there must exist a relation between the mean recurrence time and the mean moment of a repeating sequence.

[26] To test this, we convert duration magnitude into moment using the relation derived for central California earthquakes [*Bakun*, 1984]. The variation of moment with recurrence time is shown in Figure 9 together with the values found by *Nadeau and Johnson* [1998] when analyzing repeating sequences at Parkfield for smaller magnitude events. A global trend appears, not inconsistent with the $\overline{T}_r \propto M_0^{0.17}$ relation found by *Nadeau and Johnson* [1998] although there exists a strong variability and most of our measurements seem to fall behind the predicted relationship. Such a relation must imply a weak stress drop dependence with the earthquake moment, at odds with the constant mean stress drop generally observed over a large range of earthquake moments [*Abercrombie*, 1995]. The variable stress drops relation proposed by *Nadeau and Johnson* [1998] possibly leads to ~2 GPa stress drops for the smallest events. Such high stress drops are in contradiction with estimates obtained for small Parkfield earthquakes for which stress drops of the order of [1–10] MPa are found [*Imanishi et al.*, 2004]. However, the high stress drop

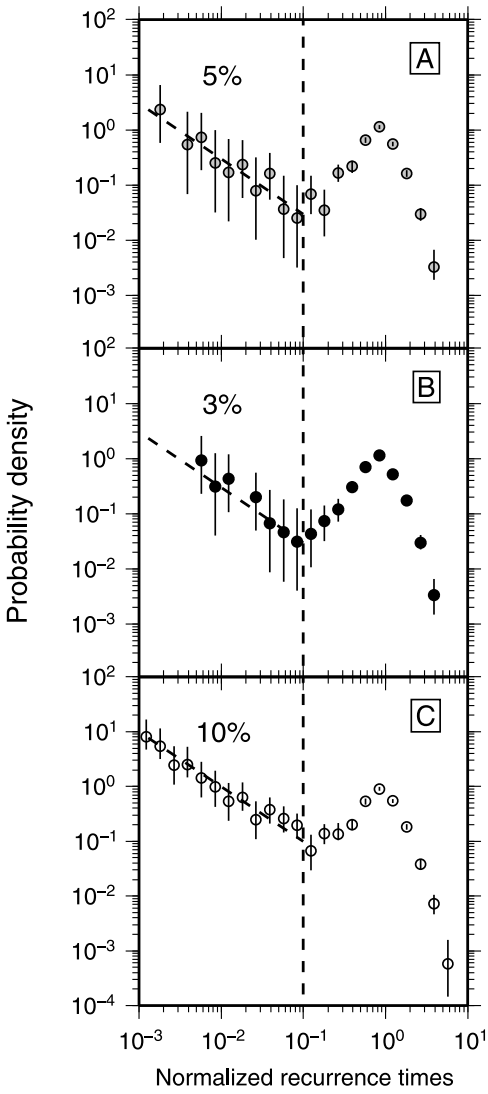

Figure 7. Probability densities for normalized recurrence times, $T_r/\overline{T}_r$, for the three sets of selection criteria. Uncertainty bars associated to each time interval are computed according to a Poisson law and represent the 90% confidence interval. The dashed line displayed between 10^{-3} and 10^{-1} is a $T_r/\overline{T}_r$ power law decay. The dashed line at 10^{-1} marks the separation between short-term triggering and periodic earthquakes; the proportion of short-term earthquakes for each selection is indicated. A peak in the distribution around 1 is observed for all selection sets. Note that the high values of the density associated with short normalized recurrence times, $T_r/\overline{T}_r < 10^{-1}$ only represent 5% of the seismicity and is, in fact, a relatively minor feature of the distribution.

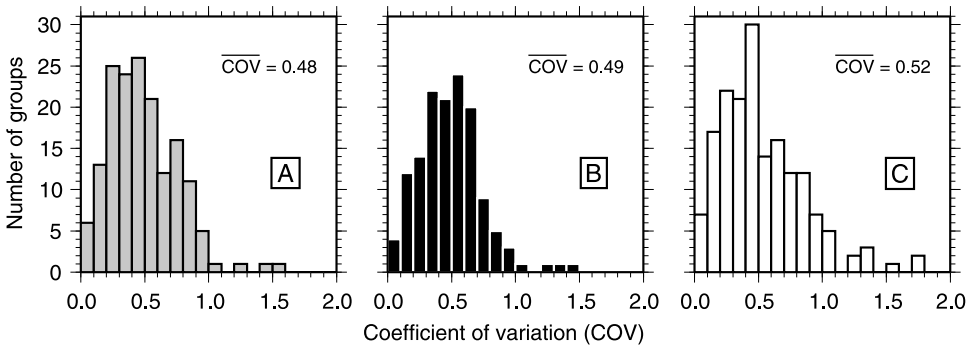

Figure 8. Histograms depicting the COV distribution for the three different set of selection criteria (a) A, (b) B, and (c) C. The mean COV is also given for each distribution. The preferred selection A has a distribution of COV similar in shape to the one obtained with a tighter approach B but contains more repeating sequences.

hypothesis results from the assumption that slip occurring on asperities is uniquely due to seismic slip. This view is not supported by an earthquake nucleation model for which aseismic slip is found to play an important role. In particular, the proportion of slip released aseismically is found to depend on the asperity size [*Chen and Lapusta*, 2009]. This eventually leads to the recurrence time vs moment scaling obtained (see Figure 9).

4.2. Short-Term Triggering

[27] We examine earthquakes that occurred at short normalized recurrence times ($T_r < 0.1 \times \overline{T}_r$) in a repeating sequence. Such short-term repeating earthquakes were already observed on the Hayward fault [*Waldhauser and Ellsworth*, 2002] and on the San Andreas fault at Parkfield [*Nadeau et al.*, 1995]. Some insight on these earthquakes can be obtained by looking at their spatial repartition relative to the barycenter of the sequence. Spatial densities of short-term and of long-term ($T_r > 0.1 \times \overline{T}_r$) earthquakes are displayed in Figure 10 for the three selection sets. Long-term earthquakes (which are mainly periodic) are tightly clustered at the barycenter of the asperity. On the opposite, short-term earthquakes occur randomly in the source area of the repeating sequence. We propose two explanations to account for this repartition:

[28] 1. Short term earthquakes are the consequence of the remaining stress left by the preceding earthquake on the same asperity. This can happen if the preceding earthquake did not rupture the entire asperity or if its slip distribution is very heterogeneous. *Dreger et al.* [2007] imaged, using an empirical Green's function deconvolution, the rupture process of a sequence of repeating earthquakes on the San Andreas fault at Parkfield. They showed that many parts of the ruptured asperity experienced high positive stress changes, even though the mean stress change on the asperity is negative.

[29] 2. A second hypothesis is that these short-term earthquakes ruptured a very close-by but distinct asperity. This idea was proposed by *Rubin* [2002] when investigating microearthquakes on the San Andreas and on the Calaveras faults: most of the earthquakes tend to occur at the edge of the rupture of the immediately preceding earthquake. They are produced by the stress concentrations induced by slip on the asperity. This explanation implies that this short-term effect is mainly due to uncertainties in the relocation process and source geometry that impact the grouping of earthquakes in repeating sequences: more accurate locations and rupture extents could indeed help discriminating these short-term earthquakes by excluding them from the sequence. Because of the supposed proximity of these short-term earthquakes to the edge of a periodic repeating sequence, even a small error in location or source geometry could cause these earthquakes to be mistakenly attached to a periodic sequence.

[30] We observe that when building repeating sequence with a looser selection C, we increase the number of earthquakes per sequence. Earthquakes are thus added to repeating sequences relative to those formed with tighter selection criteria A and B, or repeating sequences are merged. The addition of new earthquakes mostly occurs at short timescales following the occurrence of an earthquake on an asperity. The decay rate of these short-term earthquakes with time is similar to an Omori law. This power law decay is indicative of a triggering process, short-term earthquakes being probably induced by slip on a neighboring asperity.

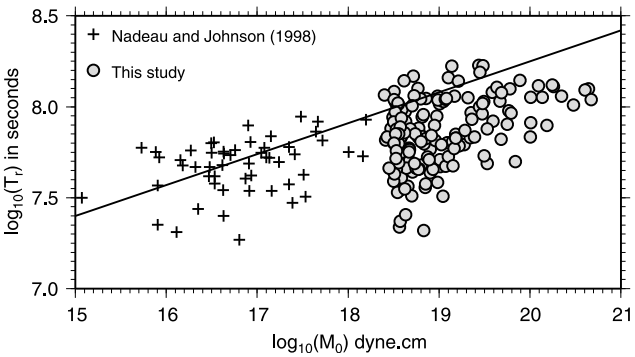

Figure 9. Variation of the mean recurrence time of a repeating sequence as a function of the mean moment of the sequence. Circles are from this study and crosses are values reported by *Nadeau and Johnson* [1998]. The line is the $\log_{10}(t) = 4.85 + 0.17\log_{10}(M_0)$ relation reported by *Nadeau and Johnson* [1998], where t is the mean recurrence time in seconds and M_0 is the mean moment of the sequence in dyne cm.

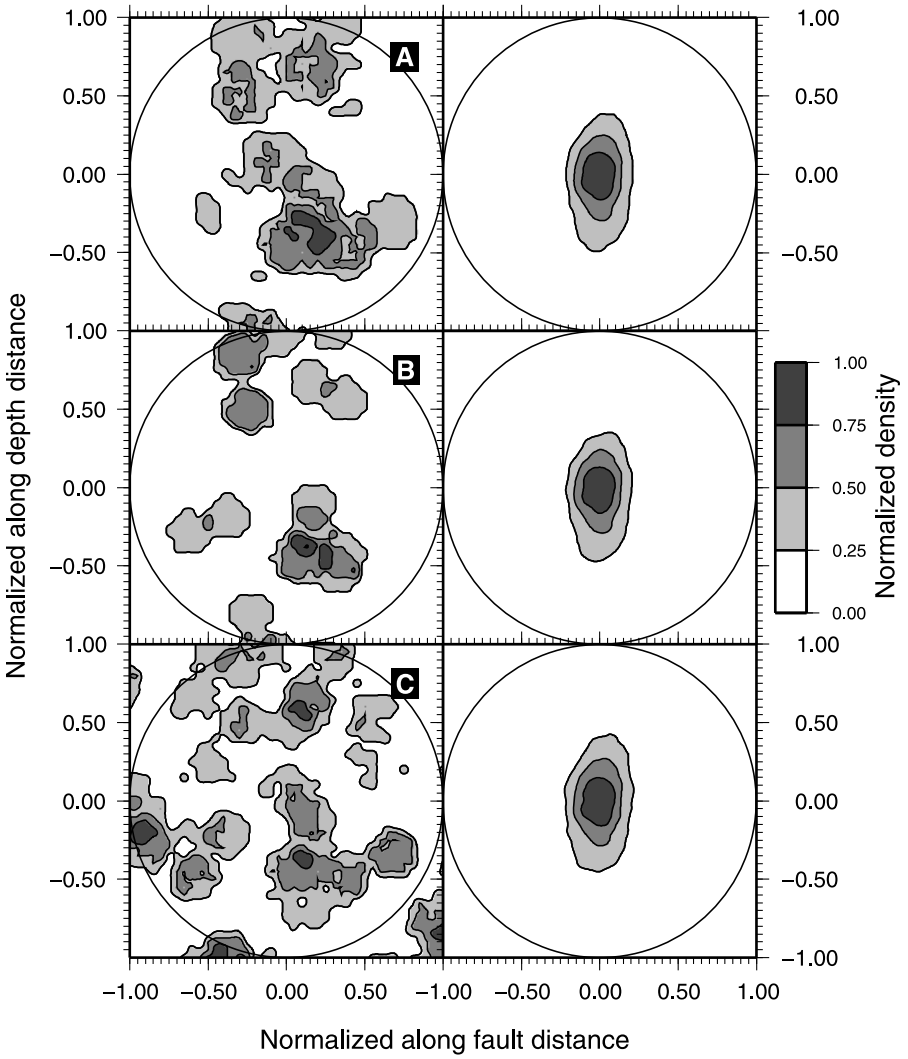

Figure 10. Spatial repartition of (left) short-term ($<0.1 \times \overline{T}_r$) and(right) long-term ($>0.1 \times \overline{T}_r$) earthquakes in a repeating sequence compared to the multiplet barycenter, for the (a) selection A, (b) selection B, and (c) selection C. Distances were normalized by the estimated rupture radius (black circle) of each earthquake, and densities were computed by stacking all the sequences. The x axis is the along strike distance, whereas the y axis is the depth. Long-term, mostly periodic, repeating earthquakes are much more clustered than short-term earthquakes, with hypocenters more or less randomly scattered around the mean rupture.

[31] When setting a tighter set of selection criteria, the periodicity of repeating earthquake sequence is not improved ($\overline{COV}$ = 0.48 for criterion A and $\overline{COV}$= 0.49 for criterion B). This is probably because in criterion B we reject earthquakes that really belong to an identified asperity but for which relocation uncertainties make them erroneously distinct from their repeaters. As the periodicity is similar, if not better, for selection A and as there is a larger number of earthquakes and repeating sequences we keep selection A as our preferred selection.

5. Perturbation Caused by the 2004 M_w = 6 Main Shock

[32] In this section we study the perturbation caused by the 2004 M_w = 6 Parkfield earthquake (hereafter denoted M6) on repeating earthquake sequences. In particular we investigate whether the periodicity is preserved or modified following the main shock by quantifying this perturbation in terms of a coseismic and postseismic stress changes, for each identified asperity.

5.1. Observations

[33] Almost all the post-Parkfield seismicity is localized in areas that also experienced earthquakes in the 1984–2004 period. At first glance it thus seems that the spatial distribution of the seismicity was not perturbed by the M6 earthquake. This conclusion was already reached by *Thurber et al.* [2006]. When looking more carefully, it appears that most post-M6 earthquakes activate asperities that were locked during the 20 previous years: among the 4026 relocated earthquakes occurring after the M6 earthquake, only 768 took place on preidentified asperities. The remaining 3258 earthquakes could not be linked to preex-

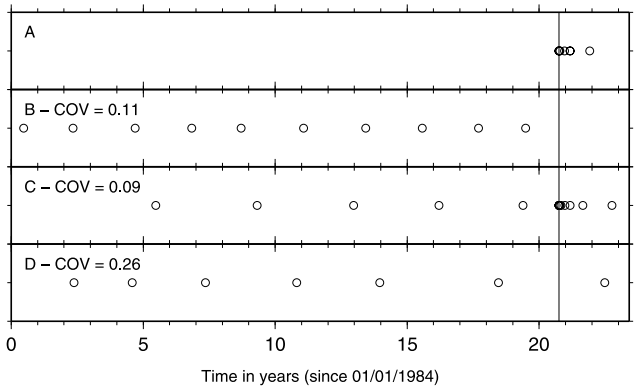

Figure 11. Examples of four identified repeating sequences A–D. Occurrence times of earthquakes repeating sequence are displayed as circles. The line at 20.7 years is the time of the 2004 $M_w = 6$ Parkfield earthquake. COV of the repeating sequences, computed in the pre-M6 interval, are displayed in top left corners. (a) Sequence A. No earthquakes occurred in the pre-M6 interval. Recurrence times increase with time after the main shock. This asperity was very likely locked since at least 1984 and then was loaded both coseismic and postseismically by the main shock. (b) Sequence B. No earthquake occurred between the Parkfield 2004 earthquake and the end time of our study in June 2007. According to the periodicity observed for the 20 previous years, an earthquake should have taken place before June 2007. This absence of such an earthquake suggests a stress unloading caused by the 2004 $M_w = 6$ Parkfield earthquake. (c) Sequence C. The robust periodicity of this sequence is greatly affected by the occurrence of the $M_w = 6$ earthquake. Numerous earthquakes occurred in a short time interval after the main shock. The recurrence times eventually increase, as expected from a typical Omori-Utsu law. (d) Sequence D. In this sequence the periodicity observed before the 2004 main shock is not significantly modified by the main shock. Figures showing waveforms for these four sequences are available in the auxiliary material.

isting repeating sequences. Among these 3258 earthquakes, 418 are organized in 87 repeating sequences with at least three earthquakes each (according to selection criterion A). An example of such a repeating sequence is displayed in Figure 11a. We do not know whether these asperities were locked or were aseismically slipping during the 1984–2004 interval. The example shown in Figure 11a is similar to the observation by *Schaff et al.* [1998], who identified repeating earthquake sequences in the aftermath of the Loma Prieta earthquake.

[34] The opposite behavior can also be observed, namely a repeating sequence identified in the 1984–2004 interval but with no earthquake occurring in the post-M6 interval. Figure 11b shows such an example with an asperity periodically failing in the pre-2004 period (low COV value of 0.11), and not rupturing any longer after the M6 earthquake, although the previous periodicity would suggest that an earthquake should have occurred there by June 2007. We will assume in our study that such an asperity has been locked by stress unloading at the time of the main shock.

[35] Two other typical asperity behaviors are illustrated in Figures 11c and 11d. These two sequences are almost perfectly periodic in the pre-M6 interval as indicated by their low COV values. However, at the time of the M6 earthquake, they gave rise to two distinct behaviors. In the first example (Figure 11c), an increased earthquake activity is observed following the M6 earthquake. This activity appears to decay with time following the main shock, similarly to what is observed in Figure 11a. Finally, in the second example (Figure 11d) we observe that a single earthquake occurred after the main shock, the periodicity noticed in the pre-M6 interval being almost preserved: the mean recurrence time is 3.2 years in 1984–2004, and 4.0 years elapsed between the last pre-M6 earthquake and the post-M6 earthquake. Figures S1–S4 showing waveforms for these four sequences (A–D) are available in the auxiliary material.[1]

[36] Despite all these different behaviors, it is remarkable to realize that adding all the repeating sequences together yield a power law, Omori-Utsu, decay for the collective dynamics (see Figure 6). While the ''building block'' (asperities) act almost deterministically, or at least in a very predictable way, when perturbed by the main shock, summing over all those very different patterns requires a purely statistical description: the collective dynamics are controlled by the variability of the perturbations affecting the asperities and are not deterministic anymore.

[37] The examples of Figure 11 show that an asperity can either be unloaded, loaded (both co and postseismically), or not significantly perturbed, by the M6 main shock. We here aim to analyze the complete population of asperities in order to investigate how these stress perturbations are spatially distributed. We distinguish three kinds of sequences: (1) type A sequences which have at least three earthquakes before M6 and no earthquake after, (2) type B sequences that have at least three earthquakes after M6 and no earthquakes before, and (3) type C sequences with at least three earthquakes in total that were active before and after M6. The spatial repartition of these three kinds of sequences shows that they are not uniformly distributed on the fault plane (Figure 12). A global trend along the strike direction is observed. Most activated sequences after the M6 earthquake are close to the hypocenter, whereas sequences that were shut down are located farther in the NW direction. In between we find most of the sequences with earthquakes both before and after M6. We also find in some areas all three types of sequences. In many places triggered sequences after the M6 earthquake are located close (a few hundred meters) to sequences that were shutdown. The observation of very different dynamical behaviors for closely located asperities strongly suggests a hight stress heterogeneity produced by the M6 earthquake on the fault plane.

5.2. Model of Coseismic and Postseismic Stress Changes

[38] All the identified asperities (i.e., repeating sequences), do not show the same dynamics in response to the M6 earthquake. This difference can be interpreted as a differ-

[1] Auxiliary materials are available in the HTML. doi:10.1029/2008JB006118.

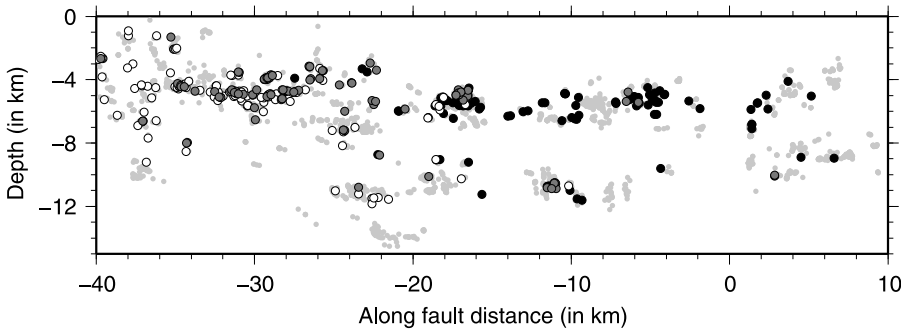

Figure 12. Cross section of the three types of repeating sequences. Black and white circles are sequences with a least three earthquakes activated only after or before the 2004 main shock, respectively, and thus correspond to positive and negative stress changes caused by the main shock, respectively. Dark gray circles are sequences with earthquakes before and after the Parkfield earthquake. Light gray circles are all relocated earthquakes in the whole time interval. The coordinate system is as Figure 4.

ence in stress changes undergone by each asperity. We propose to decompose the stress variation in two terms: (1) a coseismic stress, which effect is instantaneous, at the time of the M6 earthquake and (2) a postseismic stress, which is time-dependent. Our goal is to estimate these two stress values for each asperity, solely from earthquake occurrence times. To do this, we propose a simplified minimalist model describing the stress history on an asperity. Earthquake occurrence on an asperity is modeled as a perfectly predictable system: in the absence of any stress perturbation, the time interval between two consecutive earthquakes, T_r, is constant, as is the mean stress drop on the asperity, $\Delta\sigma_a$ (Figure 13). The perfectly predictable dynamics (i.e., periodicity) is considered valid for the whole time period preceding the 2004 M_w = 6 Parkfield earthquake. This implies that the stressing rate, for a given asperity, is constant for the whole 20 years period (1984–2004). This is the simplest model than can reproduce the observed periodicity. The mean stressing rate at an asperity can be written

$$\dot{\sigma}_a = \frac{\Delta\sigma_a}{\overline{T}_r} \tag{1}$$

At the time of the 2004 M_w = 6 Parkfield earthquake, an instantaneous coseismic stress variation, $\Delta\sigma_{co}$, is imposed by the main rupture on each asperity. This coseismic effect is then followed by a postseismic stress increase, mainly

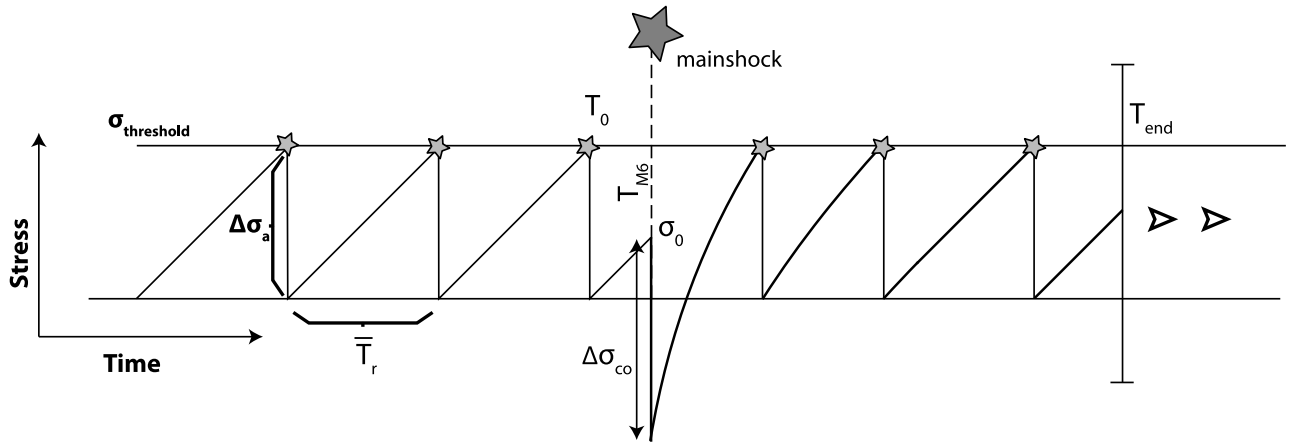

Figure 13. Sketch of the earthquake model. The stress on an asperity is represented as a function of time. It increases linearly with time before the 2004 M_w = 6 earthquake (T_{M6}). Each time the stress reaches a stress threshold $\sigma_{\text{threshold}}$, an earthquake occurs in this repeating sequence (materialized as a small star). Each failure produces a constant stress drop ($\Delta\sigma_a$) on the asperity, implying a constant recurrence time ($\overline{T}_r$) between two consecutive earthquakes in the pre-M6 interval. The last earthquake in the pre-M6 sequence occurs at time T_0. Following the M6 earthquake, an immediate coseismic stress change ($\Delta\sigma_{co}$) is applied on the asperity. This stress change can either be positive or negative. A postseismic effect, which evolves logarithmically with time, is then superimposed to the pre-M6 constant stressing rate. Earthquakes observed up to the time of our study, T_{end}, are modeled with such a stress history.

due to afterslip [*Freed*, 2007], which is time-dependent and modeled as $\sigma_{post}(t) = A \ln(t/\tau + 1)$ where t is the time following the Parkfield earthquake and A and τ are constants. This form is chosen as it empirically well reproduces the evolution of slip following the 2004 Parkfield earthquake [*Langbein et al.*, 2006; *Freed*, 2007]. Furthermore a logarithmic evolution of slip, similar to the one proposed, is also predicted by a rate and state friction model and observed for various afterslip sequences [*Marone et al.*, 1991; *Montési*, 2004; *Perfettini and Avouac*, 2004]. This postseismic effect is superimposed on the tectonic long-term stressing rate $\dot{\sigma}_a$ determined by (1). We also consider that the stress drop remains constant during the postseismic stage, equal to $\Delta\sigma_a$. Our simple threshold model gives that the sum of (logarithmic) postseismic stress increase and (constant) long-term stress rate is equal to the sum of all stress drops (stress change at asperity due to main shock plus all sequence event stress drops). It yields

$$\dot{\sigma}_a t_i + \sigma_{post}(t_i) + \Delta\sigma_{co} + \sigma_0 = n_i \Delta\sigma_a \tag{2}$$

which describes the stress of an asperity following an earthquake i rupturing this asperity. The time between earthquake i and M6 is denoted t_i and n_i is the number of post-M6 earthquakes at time t_i. The initial stress on the asperity, at the time of the Parkfield earthquake is σ_0 with

$$\sigma_0 = \frac{T_{M6} - T_0}{\overline{T}_r} \Delta\sigma_a \tag{3}$$

with T_0 the time of the last pre-M6 earthquake in the repeating sequence. We obtained after rearranging (2) and dividing by $\Delta\sigma_a$

$$n_i = \frac{t_i}{\overline{T}_r} + \frac{A}{\Delta\sigma_a} \ln\left(\frac{t_i}{\tau} + 1\right) + \frac{\Delta\sigma_{co}}{\Delta\sigma_a} + \frac{T_{M6} - T_0}{\overline{T}_r} \tag{4}$$

Equation (4) implies that the earthquake occurrence times can be used to condition the three parameters: $A/\Delta\sigma_a$, τ and $\Delta\sigma_{co}/\Delta\sigma_a$. The latter parameter is the coseismic stress change produced by the 2004 Parkfield earthquake on an asperity, normalized by the mean stress drop characteristic of earthquakes on this asperity. We work with repeating sequences with at least three earthquakes in the pre-M6 interval (after removing potential short-term earthquakes), in order to obtain an estimate of the mean recurrence time and of the initial stress on the asperity at the time of the M6 earthquake. Furthermore, we also impose the number of earthquakes in the post-M6 interval to be at least equal to 4 for resolving the three parameters using (4). We thus restrict our analysis to relatively similar sequences, discarding stress variations as the ones displayed in Figures 11a, 11b, and 11d.

[39] Parameters $A/\Delta\sigma_a$ and τ can also be resolved for asperities with earthquakes occurring only after the M6 main shock, in which case we use

$$n_i = \frac{A}{\Delta\sigma_a} \ln\left(\frac{t_i}{\tau} + 1\right) + C \tag{5}$$

instead of equation (4) since $\overline{T}_r$ is not known. The value of C in (5) is the sum of the initial stress and the stress change imposed by the main shock rupture.

6. Results

6.1. Test of a Uniform Stress Field

[40] We test whether a uniform coseismic stress or a uniform postseismic stress are compatible with the observed dynamics of earthquakes. We can first reject a uniform, both coseismic and postseismic stress over the whole fault plane as it would require all the asperities to present the same dynamics in the post-M6 time interval. This is clearly not the case, as we rather observe a diversity of behaviors (see Figure 11). We then test if a uniform postseismic stress but a variable coseismic stress is a possible model. If we set both $A/\Delta\sigma_a$ and τ to be the same for all sequences, we still face the same problem as in the previous case. We thus examine the case where $A/\Delta\sigma_a$ is allowed to vary for distinct sequences but τ is constant for all sequences. We invert the best value of τ for the 119 repeating sequences with at least four earthquakes in the post-M6 interval. We find τ = 2.5 days. Although this value of τ provides the minimum misfit for the whole set of sequences, it is rarely appropriate for describing the behavior of a particular sequence. Figures 14a and 14b show two examples for which τ is required to be variable in order to provide a reasonable explanation of the observed dynamics. A uniform τ for all sequences thus does not appear as a proper choice. This is not surprising since various τ values were found, at different surface sites, when fitting GPS and creepmeter postseismic data of the Parkfield, 2004 earthquake [*Langbein et al.*, 2006; *Helmstetter and Shaw*, 2009].

[41] A uniform normalized coseismic stress change and a variable postseismic stress cannot account for the observed behaviors. In particular, the sign of the coseismic stress change must be negative for sequences like the one displayed in Figure 11b, while it must be positive for others (e.g., Figure 14c).

[42] In Figures 14c and 14d we test a null normalized coseismic stress change on two asperities. We also perform fits of the two sequences when allowing the normalized coseismic stress to vary. The occurrence time of the first earthquake of each post-M6 sequence is mostly controlled by the coseismic stress, and cannot be well explained by the uniform coseismic stress model. In order to provide a sufficiently correct fit, one must increase the normalized coseismic stress for the first sequence (sequence C) and decrease it for the second one (sequence D). Such a discrepancy between the two sequences invalidates model that assumes a uniform coseismic stress field.

[43] Finally, keeping one of the parameter (τ or $\Delta\sigma_{co}/\Delta\sigma_a$) fixed for all sequences increases the range of inverted values for the variable parameter, as is observed in Figure 14. We thus allow both parameters to vary for each sequence, in order to correctly reproduce the evolution of seismicity on asperities.

[44] We compute the postseismic stress changes for 119 repeating sequences with at least four earthquakes in the post-M6 interval. Among these 119 sequences, 31 of them also have at least three earthquakes before the M6 earthquakes; the periodicity ($\overline{T}_r$), hence the coseismic stress

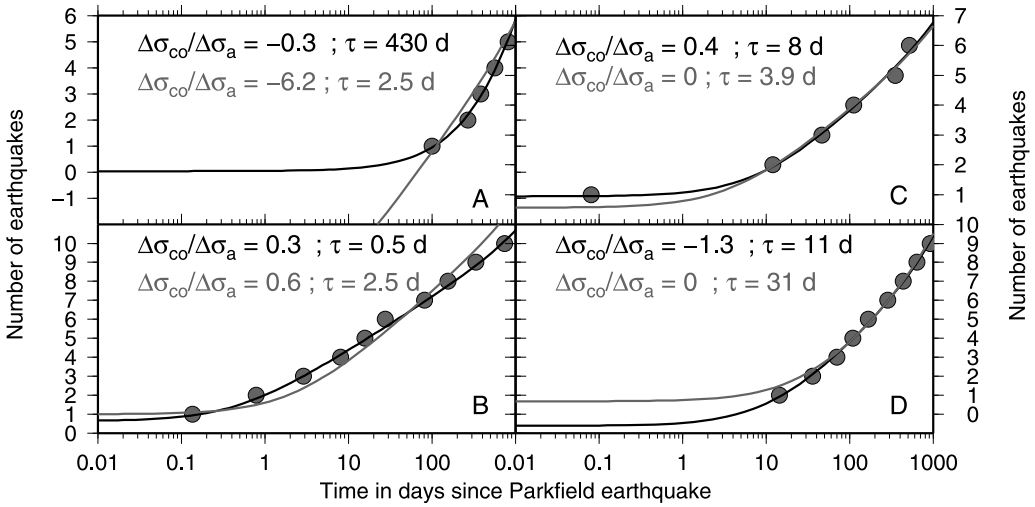

Figure 14. Evolution of the number of earthquakes on four repeating sequences as a function of time (in days) since the M6 earthquake. For each sequence the circles denote the earthquake occurrence times. The black line is the best fit of the data while the gray line is the best fit with one of the model parameter fixed. (a and b) Gray lines refer to the best fits obtained from the best value of τ inverted for the whole set of sequences. (c and d) Best fits obtained when fixing a null coseismic stress changes (gray lines).

change, can then be estimated. We display in Figure 15 the earthquake time series of four asperities among these 31. The number of occurrences is well fitted by a logarithmic function for afterslip. This is similar to the $1/t$ decay of the inverse recurrence time observed by *Schaff et al.* [1998] in repeating sequences following the Loma Prieta earthquake. Parameter uncertainties are computed from the a posteriori covariance matrix of the inversion procedure. We see in Figure 15 that parameters uncertainties (dashed lines showing the corresponding models) are anticorrelated with $\Delta\sigma_{co}/\Delta\sigma_a$. Despite a close proximity of these four repeating sequences, all located within 1 km^2, a diversity of stress changes and τ values is resolved. In particular, both negative and positive coseismic stress changes are experienced by these neighboring asperities.

6.2. Coseismic Stress Changes

[45] The main characteristic of the stress distribution is its high variability (Figure 16). As noticed in Figure 15, even closely spaced asperities may have very different stress variations. Overall, computed (normalized) coseismic stress changes range from −2.0 to 0.8. This stress distribution is very sparse, as are the locations of the repeating sequences. However, we are able to resolve stress changes with a good

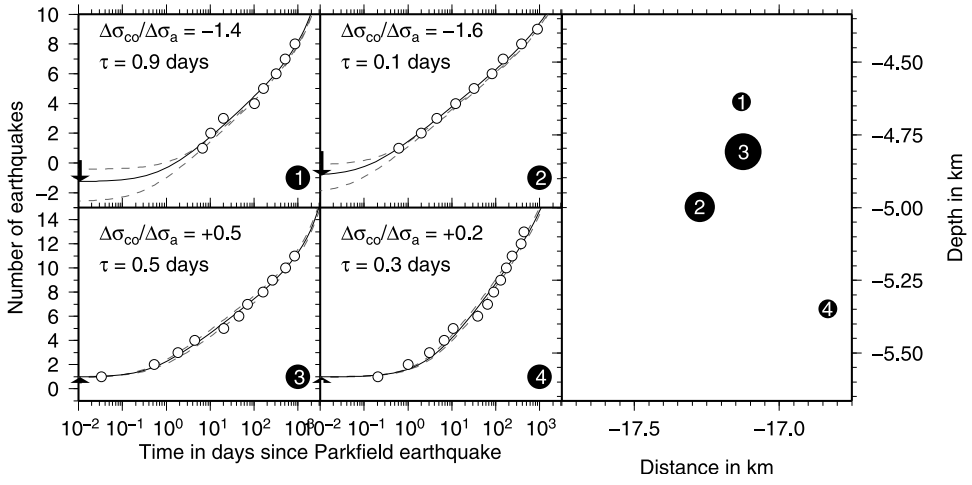

Figure 15. (left and middle) Evolution of the number of earthquakes for four repeating sequences as a function of time (in days) since the M6 earthquake (1–4). The normalized coseismic stress change, $\Delta\sigma_{co}$, and the time constant of the postseismic stress, τ, are indicated for each sequence. The black vertical arrow at the beginning of each repeating sequence shows the stress step experienced by the sequence. The curve in black shows the best model, and the two dashed curves are the 95% confidence interval. (right) A cross section showing the location of the four repeating sequences on the fault plane. The size of each circle is the approximate asperity size.

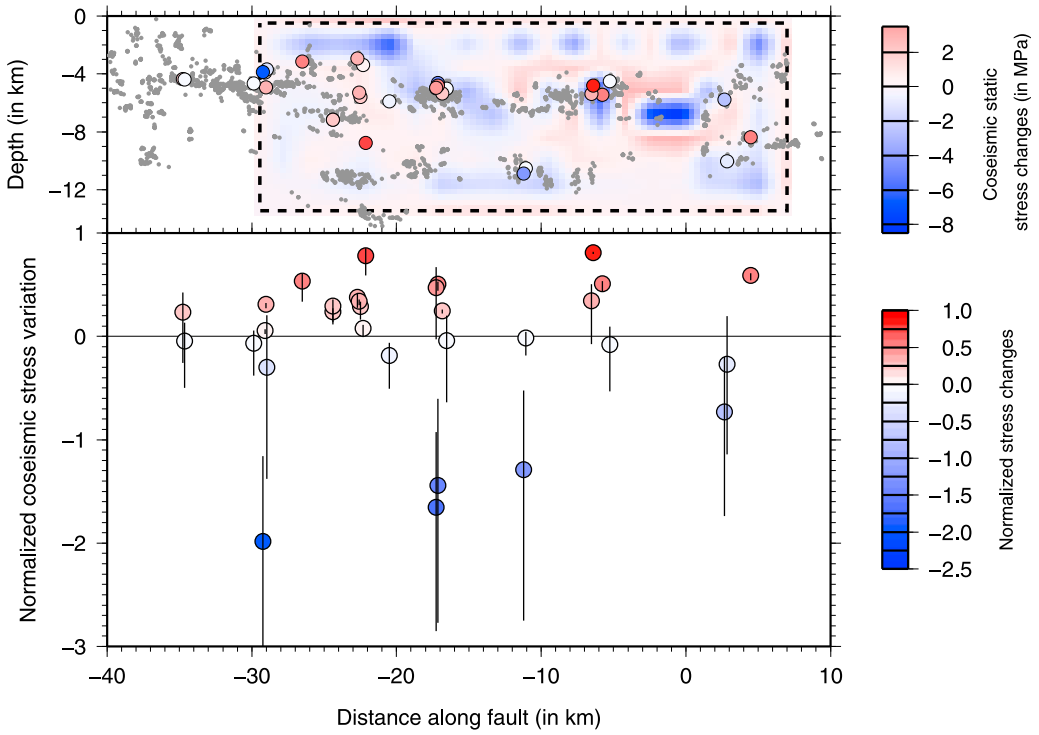

Figure 16. Normalized coseismic stress changes, function of position. (top) Cross section of all repeating sequences for which a normalized coseismic stress changes was computed. Each circle represents a distinct repeating sequence with color referring to the normalized stress change amplitudes; the circle radius is the same for all sequences. Some sequences are too close together, and cannot be all displayed. Grey dots are all relocated earthquakes. The coseismic static stress distribution, enclosed in the dashed rectangle is obtained from kinematic slip model of *Custódio et al.* [2005]. (bottom) $\Delta\sigma_{co}/\Delta\sigma_a$ function of the distance along fault.

resolution. There is no significant trend in the coseismic normalized stress change with distance along strike or depth.

[46] There neither appears any correlation between the inferred coseismic stress changes and the coseismic static stress changes derived from a kinematic slip model, as is expected if small-scale heterogeneities rather than large-scale stress indeed control aftershock occurrences (see Figure 16). Static stress changes are obtained from the static displacements inverted by *Custódio et al.* [2005] and using the wave number method of *Ripperger and Mai* [2004]. We assume an unidirectional slip and we interpolate slip on a finer grid.

6.3. Postseismic Stress Changes

[47] If only a coseismic stress change acted on each asperity, then according to a simple threshold model, the quasiperiodicity of each repeating sequence should resume after the first post-M6 earthquake of each sequence. This is clearly not the case for many repeating sequences (e.g., Figures 11a and 11c). We rather identify an abundant earthquake activity on these repeating sequences after the main shock. This may be attributed to the pronounced afterslip which is observed [*Langbein et al.*, 2006; *Freed*, 2007]. We compute the postseismic parameters $A/\Delta\sigma_a$ and τ from equation (4) for all sequences with at least four earthquakes in the post-M6 interval. Equation (5) was used instead of (4) for those sequences for which no $\overline{T}_r$ could be estimated (e.g., less than three events before the M6 earthquake). Although the postseismic stress model could be fitted to a greater number of repeating sequences than for the coseismic stress, the distribution remains sparse (Figure 17). The mean value of $A/\Delta\sigma_a$ is 1.4 and its standard deviation is 0.8. The time constant of the postseismic process is distributed over a much wider range as it spans almost 5 orders of magnitude (Figure 17), with a mean value of 1.9 days and a 95% confidence interval in [0.16; 23] days. The time constant τ can be interpreted as the time delay between the start of M6 rupture and the onset of the postseismic stress. There is thus a correlation between the total postseismic stress produced on an asperity and the value of τ, for a constant value of $A/\Delta\sigma_a$. As computed values of $A/\Delta\sigma_a$ are distributed in a narrow range compared to τ, the logarithm of the time constant is inversely proportional to the total postseismic stress experienced by an asperity. A remarkable feature of the distribution τ is the strong variation observed along the fault plane (Figure 17). These variations are observed at small scales with amplitudes higher than those associated with uncertainties. It implies that the reloading process is far from being uniform over the whole fault. It is, however, possible to distinguish a global increase of τ in the northwestern part of the fault and for the greatest depth. This is consistent with the afterslip distribution obtained using GPS [*Freed*, 2007], for which

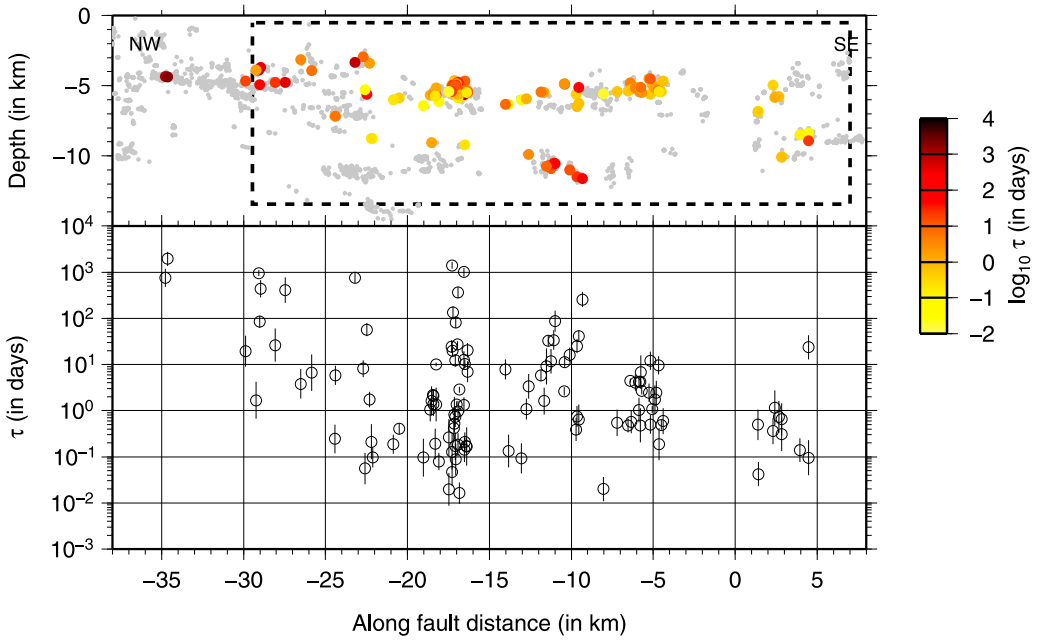

Figure 17. Same as Figure 16 but for the postseismic stress. The time constant (τ, in days) is computed for all repeating sequences with at least four earthquakes in the post-M6 interval.

most of the afterslip was localized in two shallow patches: one immediately shallower than the main shock to the southeast and the other one around 5 km depth at 15 km from the main shock to the northwest.

7. Discussion

[48] Our stress model is simplistic in many aspects and should only be seen as an end-member case. Interpretation of our results is thus limited to this particular, perfectly predictable, model. However, this simple model provides a surprisingly good description of the data. We, however, examine here its limitations and whether any of the model hypotheses could be relaxed. We first test the consequences of a possible deviation from the perfectly predictable model. For each of the 31 sequences with a normalized coseismic stress, we let the recurrence time $\overline{T}_r$ to vary in the range defined by the minimum and the maximum recurrence time of this sequence on the pre-M6 interval. This variation, well above the standard deviation, affects the initial stress on the asperity at the time of the Parkfield main shock, σ_0. However, as several sequences have their last pre-M6 earthquake close in time to the M6 earthquake, σ_0 will remain close to 0 whatever the value of $\overline{T}_r$. This perturbation of $\overline{T}_r$ leads to small deviations from the previously obtained parameters. We find a difference in normalized coseismic stress of $\pm$ 0.2 and half a decade for τ. It thus does not significantly change the distribution of our computed stress.

[49] Our assumption of a constant stress drop on a repeating sequence, $\Delta\sigma_a$, can also be challenged as it seems at odds with the apparent stress drop increase with recurrence time observed for a repeating earthquake sequences and in laboratory experiments [*Vidale et al.*, 1994; *Marone et al.*, 1995; *Marone*, 1998]. Variation of stress drop with recurrence time is interpreted as the consequence of post-main shock healing processes taking place in the fault zone. Despite seismic evidence of such an healing process taking place at Parkfield following the 2004 main shock [*Li et al.*, 2006; *Brenguier et al.*, 2008] no significant increase in stress drop was observed following the M6 earthquake for an isolated repeating sequence [*Dreger et al.*, 2007]. We thus suppose that the variation of stress drop with recurrence time, on Parkfield repeating sequences, is weak enough such that our constant stress drop ($\Delta\sigma_a$) hypothesis is reasonable.

[50] Our model compares normalized coseismic stress changes. As we do not have any information about the stress drop on asperities, $\Delta\sigma_a$, it is possible that stress drop variations among sequences act to decrease the observed heterogeneity. It could thus result that only the sign of the stress change is actually significant.

[51] Several model limitations have an effect on our computed stress distribution. First of all, because we used a threshold model, the inverted coseismic normalized stress, $\Delta\sigma_{co}/\Delta\sigma_a$, cannot exceed 1. This limits the extent of positive stress amplitude. Strong negative stress changes cannot be resolved either. This restriction is the consequence of our choice to use only sequences with at least four earthquakes in the post-M6 interval, and of the short duration of the post-M6 interval. Indeed, a strong negative coseismic stress change will cause an important delay of the first post-M6 earthquake occurrence time, which would prevent us to observe the required four earthquakes in the $\sim$2.7 years following the 2004 main shock. This restriction also applies to high values of the time constant τ. As a consequence, large positive and negative coseismic stresses cannot be resolved, and the estimation of the mean stress change is likely to be biased. It should therefore be emphasized that the computed stress changes are likely to

be much smoother than the actual stress heterogeneity experienced on the fault plane.

[52] Second, our coseismic stress inversion is very dependent on the occurrence times of early post-M6 earthquakes. Despite our detection procedure aimed at recovering short-term earthquakes missed by the NCSN catalog, it is very possible that several earthquakes were not detected. This is particularly the case for the first 30 s following the Parkfield earthquake, when the recorded signal is saturated by the main shock waveform and the coda. However, *Peng et al.* [2006] suggest that the earthquake rate following the Parkfield earthquake decays more slowly in the $\sim$30–130 s interval than at later times. If a slow decay extends down to the rupture initiation, this would downweigh the relative importance of possibly missed aftershocks. Our model could be modified to account for these missed earthquakes by allowing the coseismic stress to exceed 1, hence triggering more than just a single aftershock. This would not affect the postseismic stress inversion.

[53] We neglect in our stress model, contributions from nearby aftershocks. We show in Figure 7 that the dynamics on an asperity, during the interseismic stage, is characterized by periodicity. Unless considering that triggering from nearby earthquakes is also periodic, and with the exact same period, this suggests that only a small fraction ($\sim$5%) of earthquakes on repeating sequences are triggered events. We consider that this property is still a valid hypothesis during the postseismic stage.

[54] Finally, our stress distribution is conditioned by the location of asperities (i.e., repeating sequences): stress changes are only resolved at some locations that represent a particular kind of frictional regime, different to the rest of the fault. The large area with the largest inverted coseismic slip is mostly devoid of repeating sequences. It is possible that the stress field in this area might be smoother than the one obtained at the location of repeating sequences.

[55] The spatial resolution of our stress distribution is much better than the one usually obtained when inverting the coseismic slip from geodetic or ground motion data. Slip inversions of the 2004 M_w = 6 Parkfield earthquake, all revealed that the slip distribution (hence the stress distribution) is highly variable [*Custódio et al.*, 2005; *Johanson et al.*, 2006; *Langbein et al.*, 2006; *Liu et al.*, 2006; *Murray and Langbein*, 2006; *Custódio and Archuleta*, 2007; *Kim and Dreger*, 2008; *Ma et al.*, 2008], but they are all limited to long wavelength ($\sim$1 km). Our computed distribution of normalized coseismic stress changes, despite large uncertainties, highlights a significant heterogeneity at smaller scale. It is also possible that the stress variability extends over smaller scales than the asperity size where it was resolved (tens of meters).

[56] While the global evolution of the seismicity following the M6 earthquake is well represented by an Omori-Utsu decay (see Figure 6), as commonly observed for the majority of aftershock sequences, it is here shown to be only an average, large-scale evolution. Small-scale seismicity patterns can greatly differ from this overall evolution. Even if computed coseismic stress changes are obtained through a very simple model, and have large uncertainties, the observation of a great variety of small-scale patterns is robust. In particular, we clearly observe many cases (e.g., Figure 11c) of lowering, or even absence of seismicity following the M6 earthquake. Such decreases of seismicity, or quiescences, are rarely observed when investigated at larger scale [it *Parsons*, 2002; *Marsan*, 2003; *Felzer and Brodsky*, 2005]: the average evolution is dominated by triggering mechanisms and thus leads to the observed Omori law, even in areas where stress unloading is most common.

[57] Finally, we can also speculate on the reasons which cause significant spatial variations of τ at small scale. The initial slip speed is important in controlling the value of τ [*Marone et al.*, 1991; *Helmstetter and Shaw*, 2009]. As this initial slip speed depends on the heterogeneous coseismic slip, this can lead to a strong spatial variability of τ. Another explanation relies on the hypothesis that the normal stress on the fault is highly variable, which can be expected given the roughness of the fault plane.

8. Conclusion

[58] We show that the dynamics of repeating earthquake sequences during the interseismic stage is characterized by two distinct regimes: a short term triggering regime which accounts for a few percents of the total seismicity, and a long-term periodic recurrence. We use this periodicity to model the predicted behavior of earthquake asperities following the 2004 Parkfield, M6 earthquake. We clearly observe distinct evolutions of the repeating sequences in response to this perturbation. Although numerous sequences display an increase of activity decaying with time following the Parkfield event, some others have their activity shut down at the time of the main shock. We use a simple model to translate these perturbations of the periodicity in terms of stress changes (both coseismic and postseismic). The result highlights a significant variability of both the coseismic stress distribution and the afterslip characteristic time over the fault plane, attesting for the heterogeneous nature of the coseismic rupture and of the creep rheology. We propose that the commonly observed Omori law, describing the aftershock evolution, is a large-scale average of smaller-scale, highly variable, quasi-deterministic recurrence patterns, at least for the San Andreas fault at Parkfield.

Appendix A: Uncertainties Associated to the Probability Density Function of Figure 7

[59] This appendix details the computation of uncertainties displayed on Figure 7. For a given normalized time interval, ΔT, we call n, the number of normalized recurrence times falling in this interval and N the total number of recurrence times in all intervals. The probability that n is a result of a Poisson process of mean Λ is

$$f(\Lambda|n) = e^{-\Lambda}\frac{\Lambda^n}{n!} \tag{A1}$$

The maximum likelihood estimate (MLE) of f, is obtained for $\Lambda = \Lambda^*$. It is easily found that

$$\Lambda^* = n \tag{A2}$$

hence the MLE of the probability density for the normalized recurrence times is $n/(N \times \Delta T)$. Upper and lower bounds of

the confidence interval $(\Lambda_1;\Lambda_2)$ are then defined such that they satisfy $\Lambda_1 < \Lambda^* < \Lambda_2$ and

$$\int_{\Lambda_1}^{\Lambda_2} f(\Lambda|n)d\Lambda = I \quad \text{(A3)}$$

where I is the confidence interval. We take $I = [0.05, 0.095]$; i.e., a 90% confidence interval. The error bars, plotted on Figure 7 thus correspond to the values $\Lambda_1/(N \times \Delta T)$ and $\Lambda_2/(N \times \Delta T)$.

[60] **Acknowledgments.** We thank Michel Bouchon and Jean-Robert Grasso for discussions. We thank Jean-Luc Got for help with the relocation code and Zhigang Peng, the Associate Editor, and two anonymous reviewers for providing numerous comments that significantly improved the manuscript. Waveforms were obtained from the Northern California Earthquake Data Center (NCEDC), the Northern California Seismic Network, U.S. Geological Survey, Menlo Park, and the Berkeley Seismological Laboratory, University of California, Berkeley, for HRSN data. We acknowledge financial support from CNRS INSU program 3F. O.L. is supported by European Commission FP6 project VOLUME (contract 18471). Most of the figures were generated with the Generic Mapping Tools (GMT) [*Wessel and Smith*, 1995].

References

Abercrombie, R. E. (1995), Earthquake source scaling relationships from −1 to 5 m_L using seismograms recorded at 2.5-km depth, *J. Geophys. Res.*, *100*, 24,015–24,036, doi:10.1029/95JB02397.

Andrews, D. J. (1980), A stochastic fault model: 1. Static case, *J. Geophys. Res.*, *85*, 3867–3877, doi:10.1029/JB085iB07p03867.

Bakun, W. H. (1984), Seismic moments, local magnitudes, and coda-duration magnitudes for earthquakes in central California, *Bull. Seismol. Soc. Am.*, *74*(2), 439–458.

Bakun, W. H., and T. V. McEvilly (1984), Recurrence models and Parkfield, California, earthquakes, *J. Geophys. Res.*, *89*, 3051–3058, doi:10.1029/JB089iB05p03051.

Bakun, W. H., et al. (2005), Implications for prediction and hazard assessment from the 2004 Parkfield earthquake, *Nature*, *437*, 969–974, doi:10.1038/nature04067.

Barka, A., et al. (2002), The surface rupture and slip distribution of the 17 August 1999 Izmit earthquake (M 7.4), North Anatolian Fault, *Bull. Seismol. Soc. Am.*, *92*(1), 43–60, doi:10.1785/0120000841.

Beroza, G. C. (1991), Near-source modeling of the Loma-Prieta earthquake: evidence for heterogeneous slip and implications for earthquake hazard, *Bull. Seismol. Soc. Am.*, *81*(5), 1603–1621.

Bouchon, M. (1997), The state of stress on some faults of the San Andreas system as inferred from near-field strong motion data, *J. Geophys. Res.*, *102*, 11,731–11,744, doi:10.1029/97JB00623.

Brenguier, F., M. Campillo, C. Hadziioannou, N. M. Shapiro, R. M. Nadeau, and E. Larose (2008), Postseismic relaxation along the San Andreas fault at Parkfield from continuous seismological observations, *Science*, *321*, 1478, doi:10.1126/science.1160943.

Chen, T., and N. Lapusta (2009), Scaling of small repeating earthquakes explained by in interaction of seismic and aseismic slip in a rate and state fault model, *J. Geophys. Res.*, *114*, B01311, doi:10.1029/2008JB005749.

Custódio, S., and R. J. Archuleta (2007), Parkfield earthquakes: Characteristic or complementary?, *J. Geophys. Res.*, *112*, B05310, doi:10.1029/2006JB004617.

Custódio, S., P. Liu, and R. J. Archuleta (2005), The 2004 M_w6.0 Parkfield, California, earthquake: Inversion of near-source ground motion using multiple data sets, *Geophys. Res. Lett.*, *32*, L23312, doi:10.1029/2005GL024417.

Das, S., and C. Henry (2003), Spatial relation between main earthquake slip and its aftershock distribution, *Rev. Geophys.*, *41*(3), 1013, doi:10.1029/2002RG000119.

Dreger, D., R. M. Nadeau, and A. Chung (2007), Repeating earthquake finite source models: Strong asperities revealed on the San Andreas Fault, *Geophys. Res. Lett.*, *34*, L23302, doi:10.1029/2007GL031353.

Eshelby, J. D. (1957), The determination of the elastic field of an ellipsoidal inclusion, and related problems, *Proc. R. Soc. London, Ser. A*, *241*, 376–396, doi:10.1098/rspa.1957.0133.

Felzer, K. R., and E. E. Brodsky (2005), Testing the stress shadow hypothesis, *J. Geophys. Res.*, *110*, B05S09, doi:10.1029/2004JB003277.

Frankel, A. (1991), High-frequency spectral falloff of earthquakes, fractal dimension of complex rupture, b value, and the scaling of strength on faults, *J. Geophys. Res.*, *96*, 6291–6302, doi:10.1029/91JB00237.

Freed, A. M. (2007), Afterslip (and only afterslip) following the 2004 Parkfield, California, earthquake, *Geophys. Res. Lett.*, *34*, L06312, doi:10.1029/2006GL029155.

Got, J.-L., and P. Okubo (2003), New insights into Kilauea's volcano dynamics brought by large-scale relative relocation of microearthquakes, *J. Geophys. Res.*, *108*(B7), 2337, doi:10.1029/2002JB002060.

Got, J.-L., J. Frechet, and F. W. Klein (1994), Deep fault plane geometry inferred from multiplet relative relocation beneath the south flank of Kilauea, *J. Geophys. Res.*, *99*, 15,375–15,386, doi:10.1029/94JB00577.

Hardebeck, J. L., et al. (2004), Preliminary Report on the 22 December 2003, M 6.5 San Simeon, California earthquake, *Seismol. Res. Lett.*, *75*(2), 155–172, doi:10.1785/gssrl.75.2.155.

Harris, R. A., and P. Segall (1987), Detection of a locked zone at depth on the Parkfield, California, segment of the San Andreas fault, *J. Geophys. Res.*, *92*, 7945–7962, doi:10.1029/JB092iB08p07945.

Helmstetter, A., and B. E. Shaw (2006), Relation between stress heterogeneity and aftershock rate in the rate-and-state model, *J. Geophys. Res.*, *111*, B07304, doi:10.1029/2005JB004077.

Helmstetter, A., and B. E. Shaw (2009), Afterslip and aftershocks in the rate-and-state friction law, *J. Geophys. Res.*, *114*, B01308, doi:10.1029/2007JB005077.

Herrero, A., and P. Bernard (1994), A kinematic self-similar rupture process for earthquakes, *Bull. Seismol. Soc. Am.*, *84*(4), 1216–1228.

Hill, D. P., et al. (1993), Seismicity remotely triggered by the magnitude 7.3 Landers, California, earthquake, *Science*, *260*, 1617–1623, doi:10.1126/science.260.5114.1617.

Imanishi, K., W. L. Ellsworth, and S. G. Prejean (2004), Earthquake source parameters determined by the SAFOD Pilot Hole seismic array, *Geophys. Res. Lett.*, *31*, L12S09, doi:10.1029/2004GL019420.

Jenkins, G. M., and D. G. Watts (1968), *Spectral Analysis and Its Application*, Holden-Day, London.

Johanson, I. A., E. J. Fielding, F. Rolandone, and R. Burgmann (2006), Coseismic and postseismic slip of the 2004 Parkfield earthquake from space-geodetic data, *Bull. Seismol. Soc. Am.*, *96*(4B), S269–S282, doi:10.1785/0120050818.

Kagan, Y. Y. (2004), Short-term properties of earthquake catalogs and models of earthquake source, *Bull. Seismol. Soc. Am.*, *94*(4), 1207–1228, doi:10.1785/012003098.

Kim, A., and D. S. Dreger (2008), Rupture process of the 2004 Parkfield earthquake from near-fault seismic waveform and geodetic records, *J. Geophys. Res.*, *113*, B07308, doi:10.1029/2007JB005115.

Langbein, J., J. R. Murray, and H. A. Snyder (2006), Coseismic and initial postseismic deformation from the 2004 Parkfield, California, earthquake, observed by global positioning system, electronic distance meter, creepmeters, and borehole strainmeters, *Bull. Seismol. Soc. Am.*, *96*(4B), S304–S320, doi:10.1785/0120050823.

Li, Y.-G., P. Chen, E. S. Cochran, J. E. Vidale, and T. Burdette (2006), Seismic evidence for rock damage and healing on the San Andreas fault associated with the 2004 M6.0 Parkfield earthquake, *Bull. Seismol. Soc. Am.*, *96*(4B), S349–S363, doi:10.1785/0120050803.

Liu, P., S. Custodio, and R. J. Archuleta (2006), Kinematic inversion of the 2004 M 6.0 Parkfield earthquake including an approximation to site effects, *Bull. Seismol. Soc. Am.*, *96*(4B), S143–S158, doi:10.1785/0120050826.

Ma, S., S. Custódio, R. J. Archuleta, and P. Liu (2008), Dynamic modeling of the 2004 M_w 6.0 Parkfield, California, earthquake, *J. Geophys. Res.*, *113*, B02301, doi:10.1029/2007JB005216.

Manighetti, I., M. Campillo, C. Sammis, P. M. Mai, and G. King (2005), Evidence for self-similar, triangular slip distributions on earthquakes: Implications for earthquake and fault mechanics, *J. Geophys. Res.*, *110*, B05302, doi:10.1029/2004JB003174.

Marone, C. (1998), The effect of loading rate on static friction and the rate of fault healing during the earthquake cycle, *Nature*, *391*, 69–72, doi:10.1038/34157.

Marone, C. J., C. H. Scholz, and R. Bilham (1991), On the mechanics of earthquake afterslip, *J. Geophys. Res.*, *96*, 8441–8452, doi:10.1029/91JB00275.

Marone, C., J. E. Vidale, and W. L. Ellsworth (1995), Fault healing inferred from time dependent variations in source properties of repeating earthquakes, *Geophys. Res. Lett.*, *22*, 3095–3098, doi:10.1029/95GL03076.

Marsan, D. (2003), Triggering of seismicity at short timescales following Californian earthquakes, *J. Geophys. Res.*, *108*(B5), 2266, doi:10.1029/2002JB001946.

Marsan, D. (2006), Can coseismic stress variability suppress seismicity shadows? Insights from a rate-and-state friction model, *J. Geophys. Res.*, *111*, B06305, doi:10.1029/2005JB004060.

Marsan, D., and G. Daniel (2007), Measuring the heterogeneity of the coseismic stress change following the 1999 M_w7.6 Chi-Chi earthquake, *J. Geophys. Res.*, *112*, B07305, doi:10.1029/2006JB004651.

Montési, L. G. J. (2004), Controls of shear zone rheology and tectonic loading on postseismic creep, *J. Geophys. Res.*, *109*, B10404, doi:10.1029/2003JB002925.

Murray, J., and J. Langbein (2006), Slip on the San Andreas fault at Parkfield, California, over two earthquake cycles, and the implications for seismic hazard, *Bull. Seismol. Soc. Am.*, *96*(4B), S283–S303, doi:10.1785/0120050820.

Murray, J. R., and P. Segall (2005), Spatiotemporal evolution of a transient slip event on the San Andreas fault near Parkfield, California, *J. Geophys. Res.*, *110*, B09407, doi:10.1029/2005JB003651.

Murray, J. R., P. Segall, P. Cervelli, W. Prescott, and J. Svarc (2001), Inversion of GPS data for spatially variable slip-rate on the San Andreas Fault near Parkfield, CA, *Geophys. Res. Lett.*, *28*, 359–362, doi:10.1029/2000GL011933.

Nadeau, R. M., and L. R. Johnson (1998), Seismological studies at Parkfield VI: Moment release rates and estimates of source parameters for small repeating earthquakes, *Bull. Seismol. Soc. Am.*, *88*(3), 790–814.

Nadeau, R. M., and T. V. McEvilly (1997), Seimological studies at Parkfield V: Characteristic microearthquake sequences as fault-zone drilling targets, *Bull. Seismol. Soc. Am.*, *87*(6), 1463–1472.

Nadeau, R. M., and T. V. McEvilly (1999), Fault slip rates at depth from recurrence intervals of repeating microearthquakes, *Science*, *285*, 718–721, doi:10.1126/science.285.5428.718.

Nadeau, R. M., W. Foxall, and T. V. McEvilly (1995), Clustering and periodic recurrence of microearthquakes on the San Andreas fault at Parkfield, California, *Science*, *267*, 503–507, doi:10.1126/science.267.5197.503.

Parsons, T. (2002), Global Omori law decay of triggered earthquakes: Large aftershocks outside the classical aftershock zone, *J. Geophys. Res.*, *107*(B9), 2199, doi:10.1029/2001JB000646.

Parsons, T. (2008), Persistent earthquake clusters and gaps from slip on irregular faults, *Nat. Geosci.*, *1*, 59–63, doi:10.1038/ngeo.2007.36.

Peng, Z., J. E. Vidale, and H. Houston (2006), Anomalous early aftershock decay rate of the 2004 Mw6.0 Parkfield, California, earthquake, *Geophys. Res. Lett.*, *33*, L17307, doi:10.1029/2006GL026744.

Peng, Z., J. E. Vidale, M. Ishii, and A. Helmstetter (2007), Seismicity rate immediately before and after main shock rupture from high-frequency waveforms in Japan, *J. Geophys. Res.*, *112*, B03306, doi:10.1029/2006JB004386.

Perfettini, H., and J.-P. Avouac (2004), Postseismic relaxation driven by brittle creep: A possible mechanism to reconcile geodetic measurements and the decay rate of aftershocks, application to the Chi-Chi earthquake, Taiwan, *J. Geophys. Res.*, *109*, B02304, doi:10.1029/2003JB002488.

Ripperger, J., and P. M. Mai (2004), Fast computation of static stress changes on 2D faults from final slip distributions, *Geophys. Res. Lett.*, *31*, L18610, doi:10.1029/2004GL020594.

Rubin, A. M. (2002), Aftershocks of microearthquakes as probes of the mechanics of rupture, *J. Geophys. Res.*, *107*(B7), 2142, doi:10.1029/2001JB000496.

Rubin, A. M., D. Gillard, and J.-L. Got (1999), Streaks of microearthquakes along creeping faults, *Nature*, *400*, 635–641, doi:10.1038/23196.

Schaff, D. P., G. C. Beroza, and B. E. Shaw (1998), Postseismic response of repeating aftershocks, *Geophys. Res. Lett.*, *25*, 4549–4552, doi:10.1029/1998GL900192.

Schaff, D. P., G. H. R. Bokelmann, G. C. Beroza, F. Waldhauser, and W. L. Ellsworth (2002), High-resolution image of Calaveras Fault seismicity, *J. Geophys. Res.*, *107*(B9), 2186, doi:10.1029/2001JB000633.

Schmittbuhl, J., G. Chambon, A. Hansen, and M. Bouchon (2006), Are stress distributions along faults the signature of asperity squeeze?, *Geophys. Res. Lett.*, *33*, L13307, doi:10.1029/2006GL025952.

Sieh, K. E. (1978), Slip along the San Andreas fault associated with the great 1857 earthquake, *Bull. Seismol. Soc. Am.*, *68*(5), 1421–1448.

Thurber, C., H. Zhang, F. Waldhauser, J. Hardebeck, A. Michael, and D. Eberhart-Phillips (2006), Three-dimensional compressional wavespeed model, earthquake relocations, and focal mechanisms for the Parkfield, California, region, *Bull. Seismol. Soc. Am.*, *96*(4B), S38–S49, doi:10.1785/0120050825.

Titus, S. J, C. DeMets, and B. Tikoff (2006), Thirty-five-year creep rates for the creeping segment of the San Andreas fault and the effects of the 2004 Parkfield earthquake: constraints from alignment arrays, continuous global positioning system, and creepmeters, *Bull. Seismol. Soc. Am.*, *96*(4B), S250–S268, doi:10.1785/0120050811.

Toda, S., and R. S. Stein (2002), Response of the San Andreas fault to the 1983 Coalinga-Nunez earthquakes: An application of interaction-based probabilities for Parkfield, *J. Geophys. Res.*, *107*(B6), 2126, doi:10.1029/2001JB000172.

Vidale, J. E., W. L. Ellsworth, A. Cole, and C. Marone (1994), Variations in rupture process with recurrence interval in a repeated small earthquake, *Nature*, *368*, 624–626, doi:10.1038/368624a0.

Waldhauser, F., and W. L. Ellsworth (2002), Fault structure and mechanics of the Hayward Fault, California, from double-difference earthquake locations, *J. Geophys. Res.*, *107*(B3), 2054, doi:10.1029/2000JB000084.

Waldhauser, F., W. L. Ellsworth, D. P. Schaff, and A. Cole (2004), Streaks, multiplets, and holes: High-resolution spatio-temporal behavior of Parkfield seismicity, *Geophys. Res. Lett.*, *31*, L18608, doi:10.1029/2004GL020649.

Wessel, P., and W. H. F. Smith (1995), New version of the generic mapping tools released, *Eos Trans. AGU*, *76*, 329, doi:10.1029/95EO00198.

O. Lengliné and D. Marsan, LGIT, Université de Savoie, Campus Scientifique, F-73376 Le Bourget du Lac CEDEX, France. (olivier.lengline@univ-savoie.fr; david.marsan@univ-savoie.fr)